

A Catalog of MIPS GAL Disk and Ring Sources

D. R. Mizuno^{1,7}, K. E. Kraemer², N. Flagey³, N. Billot⁴, S. Shenoy⁵, R. Paladini³, E. Ryan⁶, A. Noriega-Crespo³, S. J. Carey³

ABSTRACT

We present a catalog of 416 extended, resolved, disk- and ring-like objects as detected in the MIPS GAL 24 μm survey of the Galactic plane. This catalog is the result of a search in the MIPS GAL image data for generally circularly symmetric, extended “bubbles” without prior knowledge or expectation of their physical nature. Most of the objects have no extended counterpart at 8 or 70 μm , with less than 20% detections at each wavelength. For the 54 objects with central point sources, the sources are nearly always seen in all IRAC bands. About 70 objects (16%) have been previously identified, with another 35 listed as IRAS sources. Among the identified objects, those with central sources are mostly listed as emission-line stars, but with other source types including supernova remnants, luminous blue variables, and planetary nebulae. The 57 identified objects (of 362) without central sources are nearly all PNe ($\sim 90\%$), which suggests that a large fraction of the 300+ unidentified objects in this category are also PNe. These identifications suggest that this is primarily a catalog of evolved stars. Also included in the catalog are two filamentary objects that are almost certainly supernova remnants, and ten unusual compact extended objects discovered in the search. Two of these show remarkable spiral structure at both 8 and 24 μm . These are likely background galaxies previously hidden by the intervening Galactic plane.

Subject headings: catalogs, infrared: ISM, planetary nebulae: general

¹Institute for Scientific Research, Boston College, 140 Commonwealth Ave., Chestnut Hill, MA, 02467-3862 USA

²Air Force Research Laboratory, AFRL/RVBYB, 29 Randolph Road, Hanscom AFB, MA 10731 USA

³Spitzer Science Center, MS 220-6, California Institute of Technology, Pasadena, CA 91125 USA

⁴Infrared Processing and Analysis Center, MS 100-22, California Institute of Technology, Pasadena, CA 91125 USA

⁵Ames Research Center, MS 245-6, Moffett Field, CA 94035 USA

⁶University of Minnesota, Department of Astronomy, 116 Church St. S.E., Minneapolis, MN 55455 USA

⁷afrl.rvb.pa@hanscom.af.mil

1. Introduction

When a star evolves up the asymptotic giant branch (AGB), its atmosphere expands and cools. The ejected gas can condense into dust grains within the circumstellar shell, which may become quite bright in the infrared (IR), while at the same time often becoming sufficiently optically thick to hide the star itself in the optical. As the star continues to evolve and shed mass, it becomes a post-AGB object, and eventually a planetary nebula (PN) or supernova (SN). These objects at the end stages of the stellar lifecycle are responsible for creating of most of the dust in the Universe (e.g. Gehrz 1989) and injecting it into the interstellar medium, where it can then form into new stars and planets. Because of the dust content of the circumstellar shells around AGB stars and in the ejecta of PNe and SNe, the IR is an ideal wavelength regime in which to identify new evolved objects. This is particularly true in the Galactic plane where high extinction in the optical limits searches to nearby sources. Previous IR surveys such as the Air Force Geophysics Laboratory (AFGL; Walker & Price 1975) and *Infrared Astronomy Satellite (IRAS)* (Olson et al. 1986) surveys found hundreds of AGB stars due to their dust emission, although they generally could not resolve the circumstellar structures around the stars.

Identification of new evolved star candidates and their circumstellar shells has recently been facilitated with the advent of high resolution mid-infrared imaging surveys. While full characterization of the progenitors may require spectroscopy, IR imaging is often the easiest and most telescope-time efficient way to identify evolved stars, particularly along lines of sight with high extinction. Specifically, the *Spitzer* Legacy surveys of the inner Galaxy, MIPS GAL (Carey et al. 2009) with the Multiband Imaging Photometer for *Spitzer* (MIPS) instrument at 24 and 70 μm (Rieke et al. 2004), and the Galactic Legacy Infrared Mid-Plane Survey Extraordinaire (GLIMPSE; Benjamin et al. 2003), with the Infrared Array Camera (IRAC) at 3.6–8.0 μm (Fazio et al. 2004), provide high resolution (1.8 to 6'') imaging of the majority of the inner Galactic disk, which should include a large fraction of the evolved stars in the Milky Way. Ring and bubble structures associated with evolved stars, PNe, and supernova remnants (SNRs) are readily identifiable in these datasets. Indeed, several studies of rings found in the GLIMPSE archive, i.e. at 3.6–8.0 μm , have already been made, such as (Phillips & Ramos-Larios 2008) or (Churchwell et al. 2006), although these were primarily from massive young stars and only a few SNRs. Here, we present a catalog of ring and disk sources found in the MIPS GAL data at 24 μm .

2. Identification of Sources

The MIPS GAL 24 μm mosaics (Mizuno et al. 2008; Carey et al. 2009) were searched by visual examination for candidate “bubble” objects. (Visual inspection is still the most reliable way to detect sets of extended objects; no automated procedure yet exists to replace the human eye.) The criteria for inclusion were: (1) Generally round shape with a hard-edged boundary; with either (2) an approximately flat “disk” profile or (3) presence of a ring or partial ring, allowing some amount of regular or irregular structure or irregular shape. In particular we excluded round and extended but centrally peaked objects: those of small angular size are either unresolved or barely resolved at the 6'' resolution of the MIPS GAL survey and thus have uncertain underlying morphology; larger, and likely resolved, examples of such objects have also been excluded from the candidate set somewhat arbitrarily. In addition to the round extended objects specifically sought, we were also attentive to any compact extended objects that had a common morphology; we identified and included an ensemble of objects that have a bipolar or “two-lobed” appearance.

A total of 416 objects were selected. The objects were grouped, by a visual assessment of their morphology, into four primary categories. The first is objects with a detected central point source at 24 μm . The objects without central point sources are separately categorized as rings, disks, or two-lobed. Each group is further divided into subgroups depending on particular symmetry and regularity properties. Note that the groups and subgroups are defined entirely by the visual appearance of the objects; we make no a priori claim that these groupings represent underlying physical distinctions apart from the obvious morphology. In addition, two small additional categories are included: filamentary objects (two items, both identified as SNRe) and a miscellaneous category (ten objects) containing singular compact extended objects.

Objects with central point sources (Group 1): The general morphology is almost invariably ringlike, which is not surprising as the visibility of a central source implies an optically thin shell. Figure 1 shows a few representative examples. The median angular size of these objects, about 44'', is approximately twice that of the objects lacking a visible 24 μm central source. Only three of objects lacking a central source are larger than 44'' (in a six times more numerous ensemble) so this difference indicates that these are a distinct population of objects apart from the visibility of the central source itself. *Regular* (1a) examples are, in gross features, axially symmetric or bilaterally symmetric. *Irregular* (1b) examples feature highly nonuniform or nonaxisymmetric ring brightness, or significant extended structure apart from the ring itself.

Rings (without central sources) (Group 2): These are divided into three subcategories.

Rings (2a) are complete rings with some allowed unevenness in ring brightness or morphology but no other significant structure. Included in this subcategory are both thin rings and the more common “thick ring” object type whose appearance is as a flat disk with a central depression. *Irregular rings* (2b) are objects featuring either a partial ring or a complete ring but with large variations in brightness or thickness around the ring. *Bilaterally symmetric rings* (2c) have an axis across which the ring has either symmetrically enhanced brightness or a change in shape such that the ring typically acquires a “D” shape on either side. Figure 2 shows examples of each of these three subcategories.

Disks (Group 3): These have five subcategories: *Flat* disks (3a) are axisymmetric, largely featureless disks with an essentially flat profile; “flat” is here assessed using a radial profile calculated for each disk from the 24 μm image data, consisting of an azimuthal average at each radius in (1".25) pixel increments, and is defined as a less than 5% drop from the peak brightness at the third pixel radius in the profiles, i.e. a region about a resolution element wide in solid angle. Some minor structure is allowed as there are no truly featureless, flat disks. *Peaked* disks (2b) are axisymmetric but fail the flatness criterion in the radial profiles. Note that circularly symmetric but strongly peaked extended objects have generally been excluded from consideration for this catalog, so this subgroup is just a partial sampling of such objects. *Bilaterally symmetric* disks (2c) have a symmetry axis with enhanced brightness on either side; typically these look like otherwise flat disks with a slot across the center. *Oblong* disks (2d) are featureless but have a slightly elliptical or elongated shape rather than round. *Irregular* disks (2e) have either pronounced asymmetric structure or irregular shape. Figure 3 shows examples of the disk subcategories. The flat and peaked examples also show horizontal profiles to demonstrate the distinction between these subgroups.

Two-lobed (Group 4): Unlike the other categories, these objects are not primarily round. Rather, they consist of two small lobes typically separated by a much fainter lane perpendicular to the emission lobes. Figure 4 shows a few examples. One lobe is usually brighter than the other, presumably due to the viewing geometry. While many of the bilaterally symmetric rings and disks have a generally two-lobed appearance, this category contains objects that have a specific two-lobed boundary and no underlying disk.

Filamentary (Group 5): This category includes localized, bounded objects with a primarily filamentary appearance, and contains just two objects which are identified as SNRs (Figure 5).

Miscellaneous (Group 6): This category contains a small number of singular compact ex-

tended objects that were discovered in the search for the disks and rings. Figure 6 shows eight of the ten; the remaining two are possible spiral galaxies and are addressed in the Appendix.

We make no claims regarding completeness of the catalog as a whole or for any of the morphology types, although an effort at a thorough visual search of all the MIPS GAL mosaics was made. Detection depends not only on the complexity and background variation of a given region of the mosaics, which are significant factors in a visual search, but also on the intrinsic properties of the sources themselves. In particular, low surface brightness objects against backgrounds with steep gradients are likely to be missed, although we have not quantified the detection problem.

2.1. Statistical overview

Of the 416 total objects, we identified 54 objects with central sources, 112 rings, 226 disks, 24 two-lobed objects, plus the two filamentary and 10 miscellaneous objects. Overall, there is slightly more than one object per square degree (~ 340 square degrees in the MIPS GAL survey), with a higher density near the Galactic center (~ 2 per square degree for $|l| < 10^\circ$) and lower away (0.85 per square degree for $l > 10^\circ$ and 0.6 per square degree for $l < 350^\circ$). The sensitivity is approximately constant over the entire MIPS GAL survey region.

Figure 7 shows a histogram of the Galactic longitude of the 240 objects with a latitude within 1° of the plane (we have data further from the plane only within 10° of the Galactic center), in 10° bins. There is a clear population enhancement in the Galactic center region, comprising about a quarter of the total, and a general falloff to larger longitudes away from the center. There are also apparent enhancements at about 30° from the center, although the small numbers make it difficult to make definite claims about the distribution. The enhancement at $l \sim 30^\circ$ is about a 2σ deviation from the general trending and is likely a real effect. The enhancement at $l \sim 330^\circ$ is only a 1σ deviation from the mean trending, and is more ambiguous.

Figure 8 shows the 2-D distribution of the objects in Galactic coordinates, separated by object group. Here all the objects are displayed. The dashed lines show the approximate boundaries of the MIPS GAL survey. The disks show a markedly higher population density at high latitude ($> 1^\circ$ from the plane) near the Galactic center, but as we have no high latitude data elsewhere, interpreting this result is problematic. Also, this increased high-latitude disk density is likely to be at least in part a selection effect as the backgrounds

at 24 μm are much more quiescent away from the plane. The rings also show a modest high-latitude enhancement but otherwise seem not to be preferentially located in the plane. The central-source objects by contrast show a definite paucity in the high-latitude data but instead show an evident clustering in regions $\sim 30^\circ$ from the Galactic center.

Figure 9 shows histograms of the angular sizes of the central-source objects, and the rings and disks combined. The lower limit of about $10''$ is dictated by the search criterion that objects be either distinctly ringlike or show a flat profile; objects much below $10''$ are either unresolved or barely resolved and thus are generally omitted from consideration due to the typical peaked appearance of such sources. All the rings and disks are below $1'$ in diameter, and the vast majority are below $30''$, while the median of the central-source objects is $44''$. The two-lobed objects are too few to provide a meaningful histogram but generally follow the rings and disks in size range.

2.2. Flux measurements

We performed aperture photometry to determine the 24 μm fluxes of the objects. For this purpose, we used both the original MIPS GAL mosaics and the point source-subtracted version of the mosaics (Shenoy et al., in preparation). For each object, an ON source radius is selected by examining both the 2-D images and 1-D vertical and horizontal slices through the center of the object. The ON radius is chosen to minimally contain the entire object.

Similarly, the 2-D images and slices are inspected to determine the radii for the OFF annulus, which are selected to match the apparent background surface brightness at the object, avoid nearby sources, and stay as close as possible to the ON radius. The background intensity I_{BG} is determined as the median of the pixels in the OFF annulus. The background is subtracted from the ON circle, the ON pixels are summed, and the sum is scaled by the pixel solid angle (for the MIPS GAL mosaics, $\Omega_{pixel} = 3.67 \times 10^{-11}$ sr) to give the flux F_{24} ,

$$\begin{aligned} F_{24} &= \Omega_{pixel} \sum_{i=1}^n (p_i - I_{BG}) \\ &= \Omega_{pixel} \left(\sum_{i=1}^n p_i - nI_{BG} \right) \end{aligned} \quad (1)$$

where the summation is over the n pixel values p_i in the ON region.

For the central-source objects, the original mosaics are used to determine the fluxes because the source subtraction is not reliable for the central sources (many are not strictly

point-like). The fluxes thus may be occasionally contaminated by other point sources occurring within the ON radius. For the remainder of the objects, and for all background measurements, the source-subtracted mosaics are used.

The flux errors are determined using both the uncertainty map (a product of the mosaic generation in the MOPEX¹ software package) and an empirically measured background error estimate. The uncertainty map provides a per-pixel error estimate ($\sigma_{UNC,i}$) and is presumed to be uncorrelated across pixels. The measurement of the RMS over the OFF annulus pixels (σ_{OFF}) reflects both pixel-to-pixel scatter and also variations that are correlated on some length scale due to true background fluctuations. To be conservative, we assume that background fluctuations dominate the OFF annulus RMS, and therefore interpret it to be the overall uncertainty in the measured background level I_{BG} assigned to the ON region, and so the error for nI_{BG} is $n\sigma_{OFF}$.

With these assumptions, the error in the flux is expressed by

$$\sigma_{F_{24}}^2 = \Omega_{pixel}^2 \left(\sum_{i=1}^n \sigma_{UNC,i}^2 + n^2 \sigma_{OFF}^2 \right) \quad (2)$$

Note that this is an upper limit because we are assuming a worst-case situation for the uncertainty in the background level measurement, which generally dominates the error expression, and also because σ_{OFF} is in part an empirical measure of some noise contributions that are already represented in the uncertainty map for the ON circle (e.g. Poisson noise from the background emission).

3. IRAC and MIPS 70 μm detections

We searched the GLIMPSE images for counterparts in each of the shorter wavelength IRAC bands, as well as the MIPS GAL 70 μm data (Paladini et al. in preparation). GLIMPSE data are available for 314 of the objects. Of these, roughly 14% (44) of the objects are detected at 8 μm with extended emission, 80% (252) were definite non-detections, and the remainder were ambiguous. At 70 μm , data are available for 368 objects, with 19% (60) detections and 46% (149) non-detections (there is a considerable amount of ambiguously associated emission at 70 μm , overlapping with the objects but with no obvious related morphology). Figure 10 shows examples of definite detections, non-detections, and ambiguous detections at 8 and 70 μm for three disk objects.

¹The MOPEX software is available for download at <http://ssc.spitzer.caltech.edu/postbcd/mopex.html>

The detection fractions are somewhat higher for the objects with $24\mu\text{m}$ central sources. The central sources themselves are observed in all IRAC bands for 94% of these objects. (IRAC central sources are observed for about 11% of the rings, disks, and two-lobed objects.) For extended emission, at $8\mu\text{m}$ (50 objects with IRAC data), there are 24% (12) detections and 56% (28) non-detections. At $70\mu\text{m}$ (46 objects), there are 43% (20) detections and 15% (7) non-detections.

Figure 11 shows three-color images of four objects using 3.6 and $8\mu\text{m}$ IRAC data from the GLIMPSE survey (blue and green) and $24\mu\text{m}$ MIPS GAL data (red). The upper left panel shows an example where there is no extended emission at $8\mu\text{m}$ (although there may be at $70\mu\text{m}$). When present, extended $8.0\mu\text{m}$ emission is typically either co-spatial (Fig. 11, upper right) with the $24\mu\text{m}$ emission or interior to it (Fig. 11, lower left). In only one instance, shown in the lower right of Figure 11, does the $8.0\mu\text{m}$ emission appear to extend beyond the $24\mu\text{m}$ structure. In this case, there is fainter emission at $24\mu\text{m}$ in the $8\mu\text{m}$ region, but the $24\mu\text{m}$ structure is dominated by the bright emission that fills the central hole in the $8\mu\text{m}$ structure. The average size of the $24\mu\text{m}$ structures that also have $8\mu\text{m}$ extended emission is $\sim 30''$. Thus, in most cases, the relative shapes and sizes of the 8 and $24\mu\text{m}$ emission regions are readily apparent.

In the cases where the 8 and $24\mu\text{m}$ emission is co-spatial, the emitting particles, presumably large molecules such as polycyclic aromatic hydrocarbons (PAHs) and small grains, respectively, must be well-mixed where the structures are well-resolved at both wavelengths (the diffraction limits were $\sim 2''$ and $\sim 6''$ at 8 and $24\mu\text{m}$, respectively), as in the examples shown in Figure 11. For the smallest disks and rings, it is harder to say, and these objects could, of course, turn out to be more complex if observed at higher resolution.

For those instances where the emission structures are clearly not co-spatial, the story is more complicated. Complex emission structures are commonly seen in the visible from planetary nebulae, such as the well-known Ring Nebula. That complexity, however, is caused by a variety of ions of different excitation potentials. Here, in a few instances where spectroscopy shows that the $24\mu\text{m}$ emission is actually line emission from [O IV], there is no detected 8 or $70\mu\text{m}$ emission, either point-like or extended (Flagey et al. in preparation). Chu et al. (2009) observed 36 known Galactic PNe with MIPS, comparing the $24\mu\text{m}$ emission with $\text{H}\alpha$ images. They explain the spatial differences between their $24\mu\text{m}$ emission and the $\text{H}\alpha$ emission as depending on the dust content and excitation/ionization structures in a particular PN. Here too, the dust density distribution and the spectral energy distribution of the central exciting source are probably also combining to create the observed 8 and $24\mu\text{m}$ emission structures. The different 'layers' of dust emission could represent different episodes of massloss from the parent star while it was on the AGB. Radiative transfer models

(e.g. Egan et al. 1988) that account for the 2- or 3-dimensional dust density structures, the spectral energy distribution of the exciting source (which will be quite problematic for the objects where none such has been detected), etc., are needed to fully describe these emission structures, as was done with *MSX* data for similar objects (e.g. Egan et al. 2002, Clark et al. 2003), but that is beyond the scope of this paper.

4. SIMBAD Correlations

To help determine the nature of these sources, we did a SIMBAD search around each object². A search radius of 2' was used to ensure that objects with imprecise coordinates, particularly IRAS sources, were not missed. The results were then compared to the 24 μm images to determine if a SIMBAD object correlated with our target or with another object in the field. We found 105 objects out of the 428 (including filamentary and miscellaneous) with a counterpart in SIMBAD. In most cases where a match was judged to be real, the SIMBAD object was within 10'' from our source coordinates. If an IRAS source corresponds to a particular section of one of our sources, such as the brightest arc of a ring, this is noted in the table notes. For the three supernova remnants, although the pulsar and other components might be closer to the center of the structure we detect, i.e. nominally a closer match to the coordinates, we give the association as the supernova remnant since we are detecting the extended emission, not the pulsar. There are a few objects that were associated with radio sources detected at a single wavelength. These cases are sufficiently unusual that they may reflect chance associations despite being within a few arcseconds of our 24 μm objects.

4.1. Morphology and Source Type

Since approximately three-quarters of our sources are unknown, we can only draw conclusions as to what they are by extension from the sources with known associations. As mentioned above, among the categories returned with the SIMBAD results is the object type. For objects that have been previously studied, a literature search may reveal further information about the object (for example, two luminous blue variables are identified simply as stars by SIMBAD). Here, we describe the kinds of previously identified objects in each of the four main categories.

²Given the updates that occasionally take place in SIMBAD we note that the searches were performed in October 2008.

Objects with central sources: Just under half (24/54) of the objects with central stars have SIMBAD counterparts, associated with either the central source or the extended emission. Eight are associated with emission-line stars, including two luminous blue variables and one post-AGB star. Two others are planetary nebulae, one is a supernova remnant, and two are identified as stars, with no further information available in the literature beyond their spectral types (B9 and M2). The remaining 11 are identified only as IRAS sources with no additional information available, except perhaps 2MASS³ data.

Rings: Of the 112 ring objects, 22 have associations in SIMBAD. Of these, over half (13) are PNe, distributed fairly evenly among the three ring subgroups (given the small numbers involved). Six more are IRAS sources, two are radio wavelength objects, and one is a B9 star. As with the central star objects, these 9 have no additional references.

Disks: The SIMBAD associations among the 226 disk objects are predominantly planetary nebulae: 36 of the 42 objects with counterparts are PNe. The remainder include three otherwise anonymous IRAS sources, two radio wavelength objects, and one eclipsing binary.

Two-lobed: Only five of the thirty two-lobed objects have SIMBAD counterparts. Two are PNe identified in the Macquarie/AngloAustralian Observatory/Strasbourg H α planetary nebula survey (Parker et al. 2006; Miszalski et al. 2008). Two have an IRAS association with no other information available. The last is associated with a star in the young open cluster NGC 6383, and as with the small number of radio sources, may be a chance spatial coincidence.

5. The catalog

Table 1 is the catalog of all the objects. The table is divided into object group and subgroups, and within each subgroup the objects are sorted by increasing Galactic longitude.

Name: Constructed on the Galactic longitude and latitude.

³Most MGE sources have at least one 2MASS source within 5'', often more than one, which is not surprising given the density of sources in the Galactic plane. However, unless there is corresponding point source at IRAC wavelengths, a chance alignment cannot be ruled out.

J2000 Coordinates: The centers of the objects were selected by eye and specified as the nearest pixel in the MIPS GAL mosaics, so the precision for the coordinates is good to about $2''$.

Diameter: The boundaries of the objects are evaluated by eye in the mosaics, and the diameter on the horizontal axis (for round objects) is specified as the nearest integral pixel span, converted to arcseconds and rounded to integral values. For objects with irregular boundaries, the larger of the horizontal and vertical axes is used.

$24\ \mu\text{m}$ flux: As described in Section 2.2. The errors calculated from equation (2) are shown as percentages. Errors greater or equal to 100% are truncated to 99%.

Detection flags: These are determined by visual inspection of the $8\ \mu\text{m}$ GLIMPSE images and $70\ \mu\text{m}$ MIPS GAL images. For point sources, an affirmative result (“Y”) required a point source at the geometric center of the object and be free of confusion. An ambiguous result (“?”) is indicated if a source is slightly off-center or there is confusion present. A negative result (“N”) means clearly no point source present. A dash means no data are available. For extended emission, an affirmative result required a morphology similar to the $24\ \mu\text{m}$ morphology (or at least concentric), an ambiguous result means some local extended emission present but of uncertain correspondence to the $24\ \mu\text{m}$ emission, and a negative result means either no localized extended emission present or emission that is clearly not associated with the object.

SIMBAD associations: These columns show the SIMBAD associations as described above. In about a dozen cases, two probable associations are present, typically a planetary nebula coincident with our coordinates, plus an IRAS source that is almost certainly the same object but has not been noted as such in SIMBAD. In these cases the primary identification is given as the planetary nebula or star, and the IRAS association is indicated in a footnote. Five objects were matched with separate searches in the catalogs in the VizieR service which are not yet incorporated into SIMBAD; these are noted in footnotes.

6. Discussion

While spectroscopic study would be necessary to determine the physical nature of any given object, we may draw some tentative conclusions based on the known identifications. It is striking that for the rings, disks, and two-lobed objects, nearly all of the specific SIMBAD identifications (50 of 57) are either PNe or PN candidates, and the remainder are identified as either stars or radio sources, which does not preclude these objects from being PNe as

well. The objects in the catalog have been selected solely on the basis of their $24\ \mu\text{m}$ morphology, and without prior knowledge or expectation of what any of these objects are, so it is tempting to conclude from the near-universality of the PN identifications that the ring, disk, and two-lobed lists collectively form a catalog of PNe in the MIPS GAL survey region, specifically PNe that are both observed and resolved at the $6''\ 24\ \mu\text{m}$ MIPS resolution.

This catalog could therefore contain up to 300 previously undiscovered PNe, helping to alleviate the known discrepancy between the number of expected Galactic PNe and the number that have been identified (e.g. Parker et al. 2003; Phillips & Ramos-Larios 2008), which can, at least in part, be attributed to extinction effects that are largely absent at $24\ \mu\text{m}$. It is also possible, however, that the unidentified objects are located preferentially deeper in the Galactic disk, and some portion of them may be massive evolved stars or other object types observed from a great distance rather than garden-variety PNe.

The completeness of this tentative PN catalog (rings, disks, and two-lobed objects) is limited by the general exclusion of centrally peaked objects, whether the selection of “irregular” objects encompasses the actual range of morphological PN variation, and the vagaries of a visual search of a large image set. PNe can be strongly peaked at $24\ \mu\text{m}$; see Su et al. (2004) for an example that most likely would have been excluded from our catalog for that reason. Of the 35 “peaked” disks in the list, all 7 with identifications are PNe, so this suggests that there are many more such objects that have been omitted from the catalog. Circularly symmetric, centrally peaked extended objects are perhaps 10-15 times more numerous in the MIPS GAL data than the rings and disks selected for this catalog, but this larger ensemble certainly includes objects such as YSOs (see, e.g., Cyganowski et al. 2008 for some examples) and unresolved sources at $24\ \mu\text{m}$.

In contrast to the ubiquitous identification of the ring and disk objects as PNe, Morris et al. (2006) present an outer Galaxy object discovered in the *Spitzer* Galactic First Look Survey morphologically similar at $24\ \mu\text{m}$ to the objects selected for this catalog (we would categorize it as an irregular ring). Spectroscopy showed that this object lacks a dust continuum; virtually all the $24\ \mu\text{m}$ emission is attributed to [O IV]. These authors interpret this object as a young supernova remnant. This object is slightly larger in angular extent, about $1'$, than the largest of our rings and disks, but not enough to argue that it is in a separate class of objects. In other gross properties (low surface brightness, lack of detection in IRAC bands and $70\ \mu\text{m}$) it is similar to many of our ring and disk objects. Spectroscopic data for one of our irregular ring objects, MGE059.4354-00.4662, also shows a lack of a dust continuum (Billot et al. 2009), and whose $24\ \mu\text{m}$ signature is also due to ionized oxygen.

Chu et al. (2009) compared MIPS $24\ \mu\text{m}$ observations of Galactic PNe with archival H α and He II data. They suggest that the $24\ \mu\text{m}$ emission is a combination of dust continuum

emission and the [O IV] line at $25.9 \mu\text{m}$, where the relative contributions depend on the ionization and dust density structure of the PN in question. Additional *Spitzer*Infrared Spectrometer (IRS) (Houck et al. 2004) observations of a small sample of ring and disk sources will help determine the emission mechanisms in the present catalog (N. Billot et al. in preparation, N. Flagey et al. in preparation).

The objects with central sources form an ensemble distinct from the sourceless rings and disks. While two are identified as candidate PNe, the majority of the identifications (apart from the generic IR sources) are that of the central stars, and a preponderance of these are emission-line stars.

While the visibility of the residual star in a PN at $24 \mu\text{m}$ is generally not anticipated, Su et al. (2007) report a bright central pointlike source at $24 \mu\text{m}$ in the Helix nebula, which they attribute to an unresolved debris disk surrounding the white dwarf. The two identified central-source PNe candidates in our catalog fall in the angular size range of the rings and disks, and so this could be a plausible interpretation for the smaller of the unidentified central-source objects, but the majority of the central-source objects have a significantly larger angular size than even the largest rings and disks (or identified PNe among them), and so this interpretation should not be assumed for the central-source objects in general without further evidence. (A debris disk model is more likely for the peaked disks in our catalog.)

We therefore attempt no general interpretation of the central-source objects except to speculate that they are all evolved objects. One interesting characteristic is their Galactic distribution: the apparent clustering at 30° from the Galactic center corresponds to the tangent points of the molecular ring. If these objects are largely confined to the molecular ring then this suggests that they are evolved stages of massive, short-lived stars.

This work is based on observations made with the *Spitzer* Space Telescope, which is operated by the Jet Propulsion Laboratory, California Institute of Technology under a contract with NASA. Support for this work was provided by NASA in part through an award issued by JPL/Caltech. This research made use of the SIMBAD database and the VizieR catalog access tool, operated by the Centre de Données Astronomiques de Strasbourg. This research has also made use of NASA’s Astrophysics Data System Bibliographic Services.

A. Two possible new spiral galaxies

As mentioned in the main text, in addition to the sources with a strong degree of circular or bipolar symmetry, we also noted a number of other unusually shaped objects. Of particular note are the two objects shown in Figure 12. Each shows remarkable spiral structure at both 24 and 8 μm ; neither has a counterpart found in SIMBAD.

For MGE314.2378+00.9793, the extended ($\sim 45 \times 80''$ at 24 μm) spiral emission is prominent at 24 and 8 μm , and faintly visible at 5.8 μm . The central region appears dominated by 3.6 μm emission, although there is a central point source present in all 5 bands. In contrast, the central region of MGE351.2381-00.0145 is dominated by a blob of 24 μm emission ($\sim 13''$) that is completely absent at the shorter wavelengths. The spiral structure, $\sim 75''$ across at 24 μm , is detected at 5.8 as well as 8 and 24 μm . There also appears to be 70 μm emission associated with MGE351.2381-00.0145.

One possibility is that these are two spiral galaxies previously hidden due to their location behind the Galactic plane. This seems particularly plausible for MGE351.2381-00.0145, located at $(l,b) = (351.24, -0.01)$; MGE314.2378+00.9793 is at a slightly higher latitude, $(l,b) = (314.24, +0.99)$, but still well within the plane. Both are in rich star fields, as evidenced by the numerous 3.6 μm sources in the figure. MGE314.2378+00.9793 coincides with an 843 MHz radio continuum source from the Sydney University Molonglo Sky Survey (Bock et al. 1999), and MGE351.2381-00.0145 has a radio continuum source at 1.4 GHz from the NRAO VLA Sky Survey (NVSS, Condon et al. 1998). The location of MGE314.2378+00.9793 is also coincident with the Norma Wall of galaxies, about a degree from the two galaxies recently found with IRAC by the GLIMPSE team (Jarrett et al. 2007). (Those two galaxies, MGE316.8732-00.5991 and 317.0392-00.4974, are actually two of the three objects in the “miscellaneous” group with SIMBAD associations.) Follow-up observations to determine their radial velocities would be necessary to test this scenario for the two spiral sources.

A second possibility for MGE314.2378+00.9793 is that there are two rings superimposed, with one rotated about 30° . One trouble with this, though, is that while there is a point source reasonably well-centered in the overall structure, there do not seem to be point sources near the center of either of the potential separate ring structures.

An alternative explanation for MGE351.2381-00.0145 is some kind of rotating wind mechanism, creating a pinwheel nebula comparable to that around Wolf-Rayet stars such as WR 104 (Tuthill et al. 1999) or WR 98a (Monnier et al. 1999). The lack of a point source at the center does not really support that, though, as well as the fact that the angular size of the MGE351.2381-00.0145 nebula, several hundred times the $\sim 0''.2$ of WR 104, makes the WR interpretation unlikely. On the other hand, we know of no spiral galaxies with such

strong central emission at $24\ \mu\text{m}$ yet not at $8\ \mu\text{m}$.

Another “miscellaneous” object, MGE356.3395+02.0502, shown in Figure 6, is a central point source with a bright bar of emission plus a fainter halo above and below the bar. It, too, is an NVSS point source, and could be a smaller or more distant spiral seen edge-on, rather than face-on as with the first two objects. Unfortunately, at (l,b) \sim 356.34, 2.05, it was outside the GLIMPSE coverage. Again, additional observations are needed to determine what this source actually is.

MGE305.3881+00.0804 has a morphological similarity to photoablating proplyd candidates observed at optical wavelengths in Orion (O’Dell et al. 1993) and the Carina Nebula (Smith et al. 2003). The Wolf-Rayet star WR 48a is about $2'$ distant and is approximately aligned with the head-tail orientation of this object. At a distance of 4 kpc, the $\sim 1'$ tail is ~ 1 pc in length, ~ 100 times that of the Orion proplyds and ~ 10 times those in Carina, which suggests that this could be a much more massive protoplanetary disk than those found in Orion or Carina.

MGE003.7032-01.7927 resembles a proplyd, but there is no apparent source driving the flow. A jet could be a possibility, but this is nothing like a YSO protostellar jet, and there is no signature of a counter-jet.

REFERENCES

- Benjamin, R. A., et al. 2003, *PASP*, 115, 953
- Billot, N., Flagey, N., Noriega-Crespo, A., Shenoy, S., Mizuno, D., Kraemer, K., & Latter, B. 2009, *BAAS*, 214, 316.05
- Bock, D. C.-J., Large, M. I., & Sadler, E. M. 1999, *AJ*, 117, 1578
- Carey, S. J., et al. 2009, *PASP*, 121, 76
- Chu, Y.-H., et al. 2009, *AJ*, 138, 691
- Churchwell et al. 2006, *ApJ*, 649, 759
- Clark, J. S., Egan, M. P., Crowther, P. A., Mizuno, D. R., Larianov, V. M., & Arkharov, A. 2003, *A&A*, 412, 185
- Condon, J. J., Cotton, W. D., Greisen, E. W., Yin, Q. F., Perley, R. A., Taylor, G. B., & Broderick, J. J. 1998, *AJ*, 115, 1693
- Cyganowski, C. J., et al. 2008, *AJ*, 136, 2391
- Egan, M. P., Clark, J. S., Mizuno, D. R., Carey, S. J., Steele, I. A., & Price, S. D. 2002, *ApJ*, 572, 288
- Egan, M. P., Leung, C. M., & Spagna, G. F. Jr. 1988, *Comput. Phys. Commun.*, 48, 271
- Fazio, G., et al. 2004, *ApJS*, 154, 10
- Gehrz, R. D. 1989, in *IAU Symp. 135, Interstellar Dust*, Ed. L. J. Allamandola & A. G. G. M. Tielens (Dordrecht: Kluwer), 445
- Helfand, D. J., Becker, R. H., White, R. L., Fallon, A., & Tuttle, S. 2006, *AJ*, 131, 2525
- Houck, J., et al. 2004, *ApJS*, 154, 18
- Jarrett, T. H., et al. 2007, *AJ*, 133, 979
- Miszalski, B., Parker, Q. A., Acker, A., Birkby, J. L., Frew, D. J., & Kovacevic, A. 2008, *MNRAS*, 384, 525
- Mizuno, D. R., et al. 2008, *PASP*, 120, 1028
- Monnier, J. D., Tuthill, P. G., & Danchi, W. C. 1999, *ApJ*, 525, L97

- Morris, P. W., et al. 2006, *ApJ*, 640, L179
- O’Dell, C. R., Wen, Z., & Hu, X. 1993, *ApJ*, 410, 696
- Olton, F. M., & Raimoud, E. 1986, *A&AS*, 65, 607
- Parker, Q., et al. 2003, in *IAU Symp. 209, Planetary Nebulae: Their Evolution and Role in the Universe*, ed. S. Kwok, M. A. Dopita, & R. Sutherland (San Francisco: ASP), 25
- Parker, Q. A., et al. 2006, *MNRAS*, 373, 79
- Phillips, J. P., & Ramos-Larios, G. 2008, *MNRAS*, 386, 995
- Rieke, G., et al. 2004, *ApJS*, 154, 25
- Smith, N., Bally, J., & Morse, J. 2003, *ApJ*, 587, L105
- Su, K. Y. L., et al. 2004, *ApJS*, 154, 302
- Su, K. Y. L., et al. 2007, *AJ*, 657, L41
- Tuthill, P. G., Monnier, J. D., & Danchi, W. C. 1999, *Nature*, 398, 487
- Walker, R., & Price, S. D. 1975, *AFCRL-TR-75-0373*
- White, R. L., Becker, R. H., & Helfand, D. J. 2005, *AJ*, 130, 586

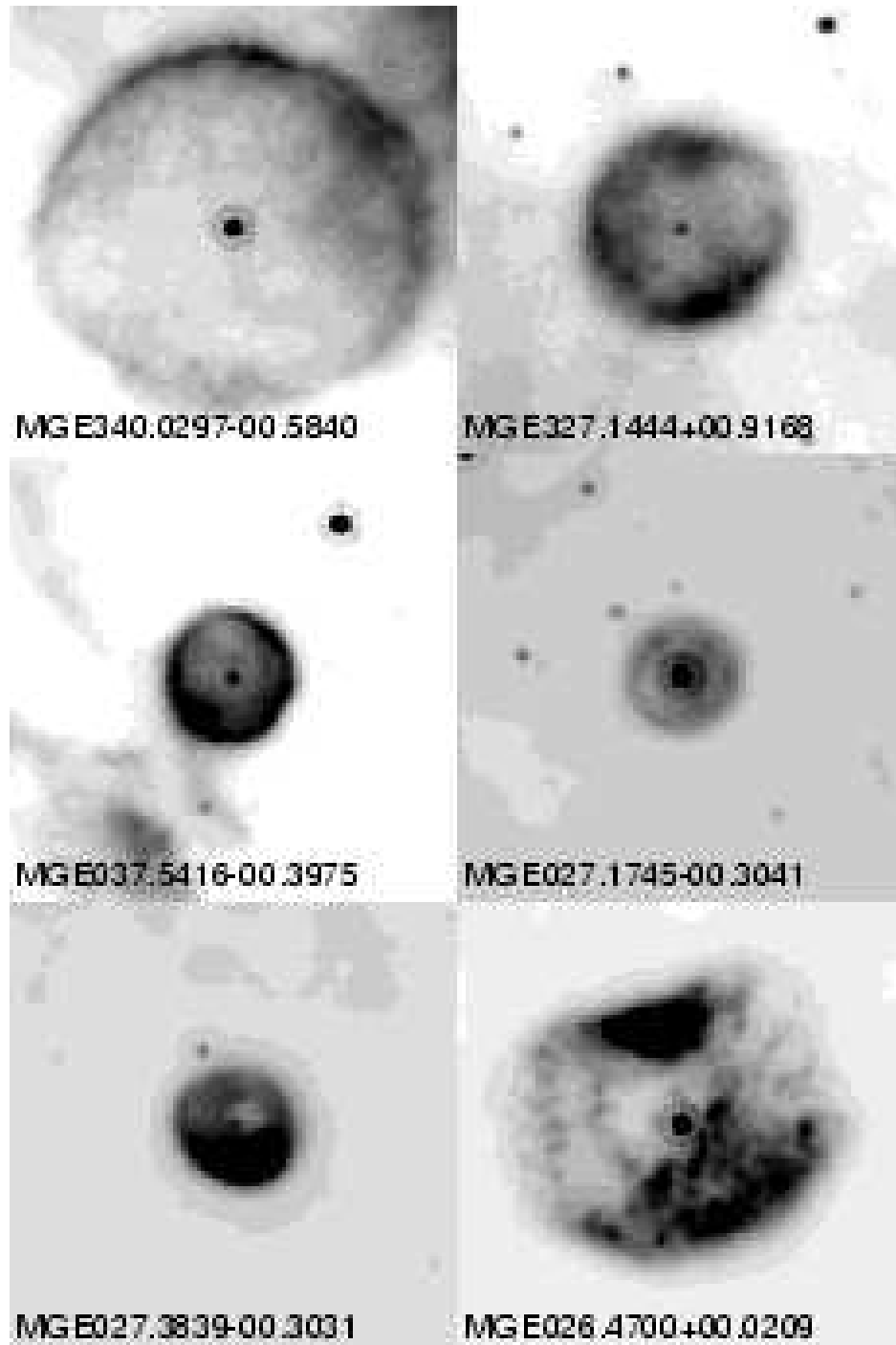


Fig. 1.— Examples of objects with central sources. The bottom row are “irregular” examples. Each panel is about $3'.3$ across.

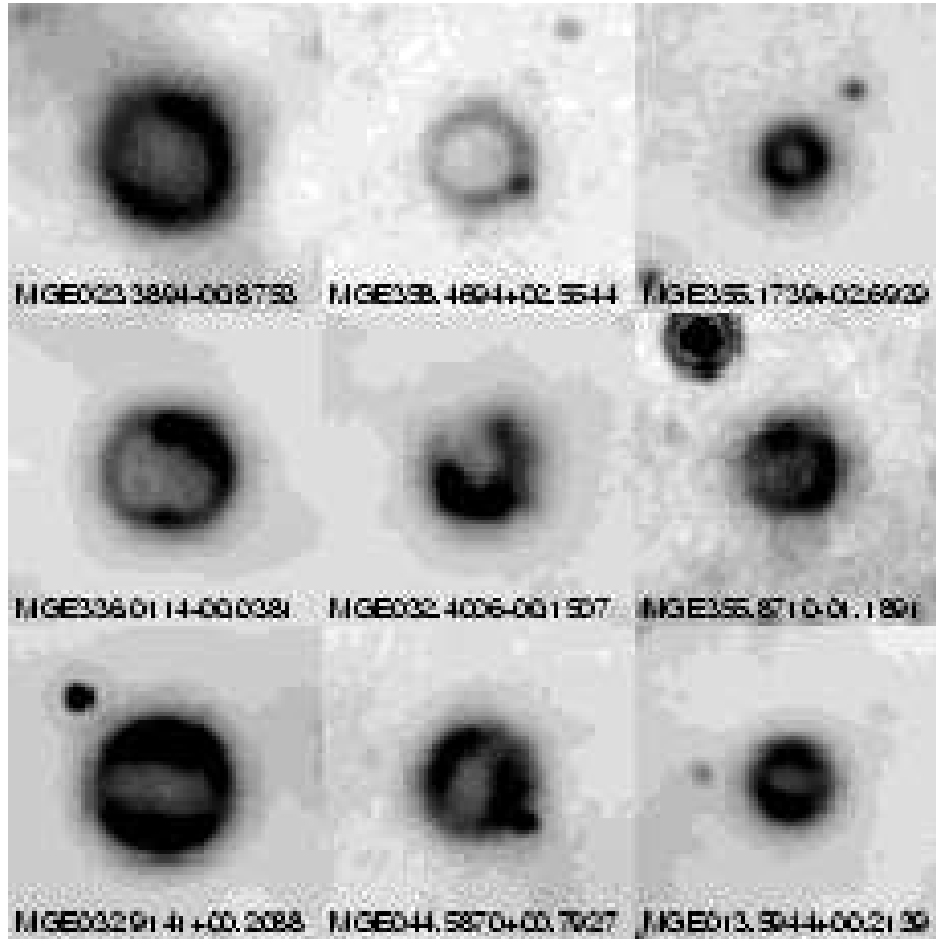


Fig. 2.— Examples of ring objects. Top row: Rings. Middle: Irregular rings. Bottom: Bilaterally symmetric. Each panel is about $1'.5$ across.

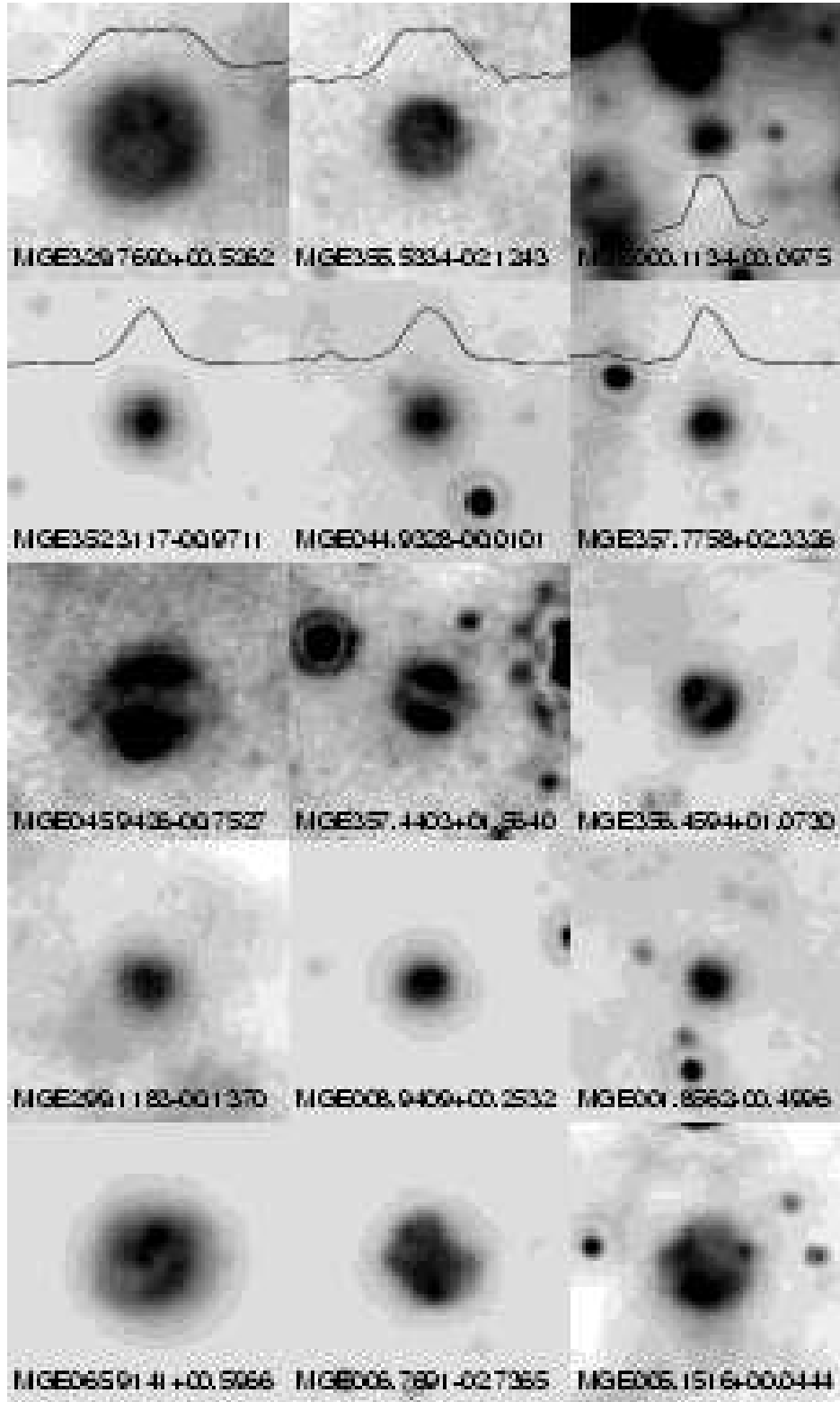


Fig. 3.— Examples of disk objects. Top to bottom: flat, peaked, bilaterally symmetric, oblong, and irregular. Each panel is about $1/5$ across. The flat and peaked examples also have horizontal slices included to show the distinction between these subgroups.

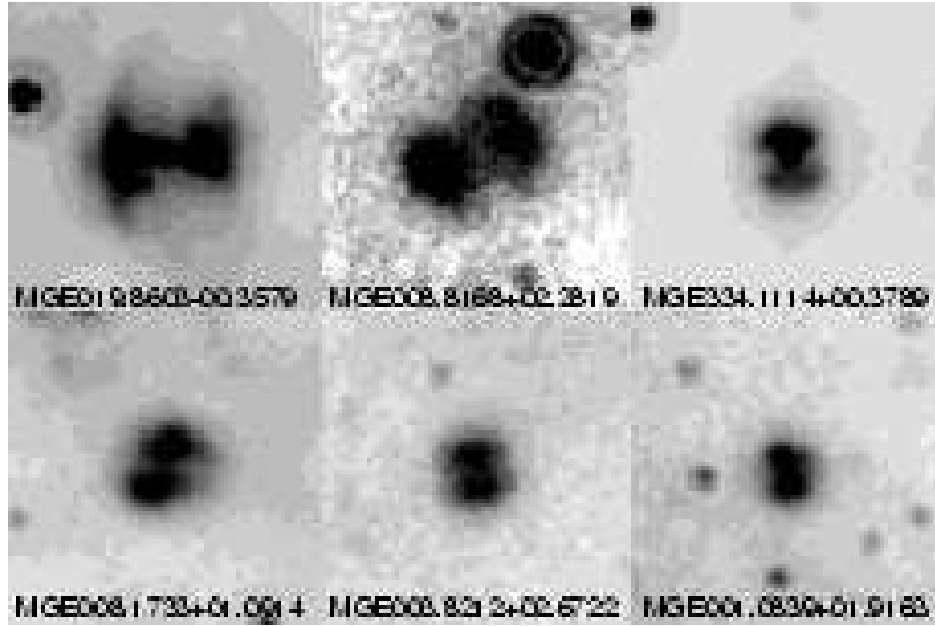


Fig. 4.— Examples of two-lobed objects. Each panel is about $1'.5$ across.

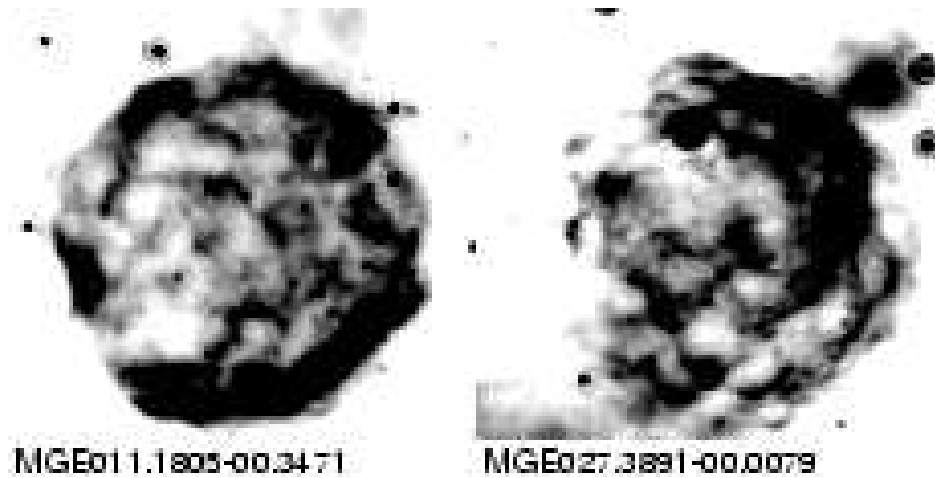


Fig. 5.— Filamentary objects. Each panel is about $5'.6$ across.

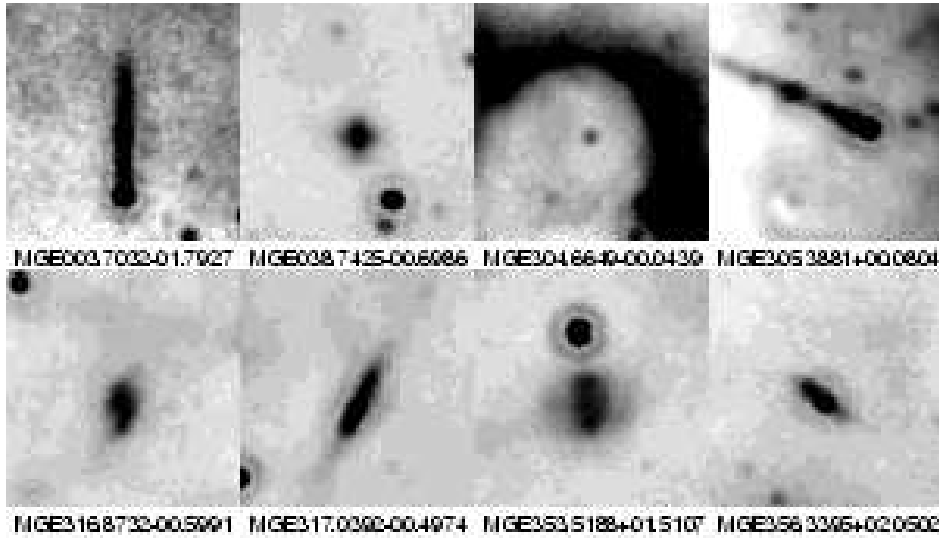


Fig. 6.— Miscellaneous objects. Each panel is about $1'.5$ across. MGE316.8732-00.5991 and MGE317.0392-00.4974 are galaxies identified in the GLIMPSE survey (Jarrett et al. 2007).

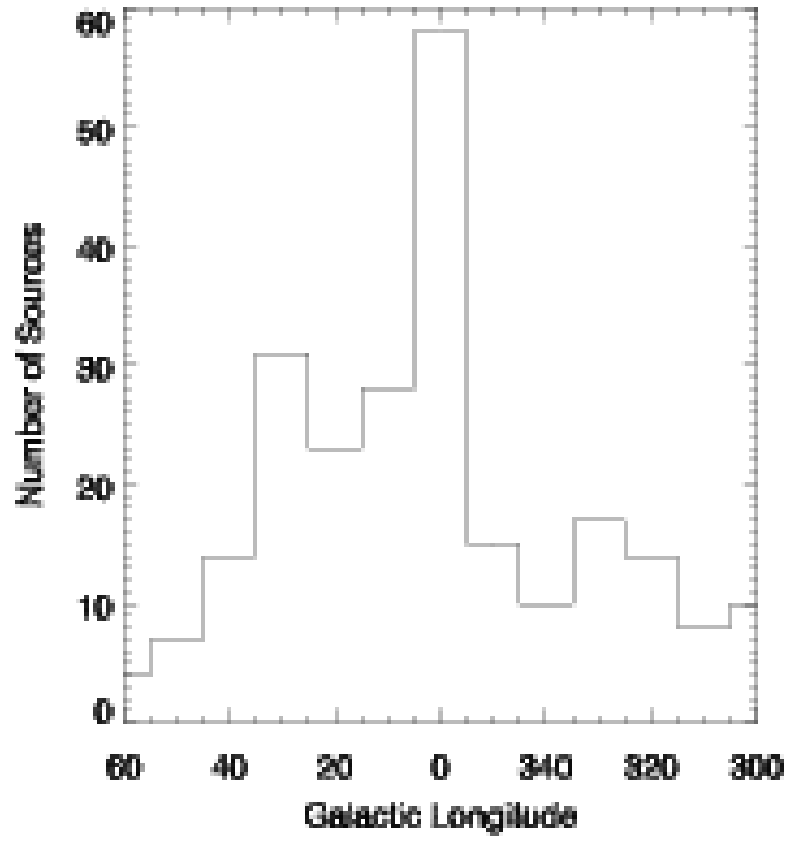


Fig. 7.— Histogram of Galactic longitudes of objects within 1° of the plane.

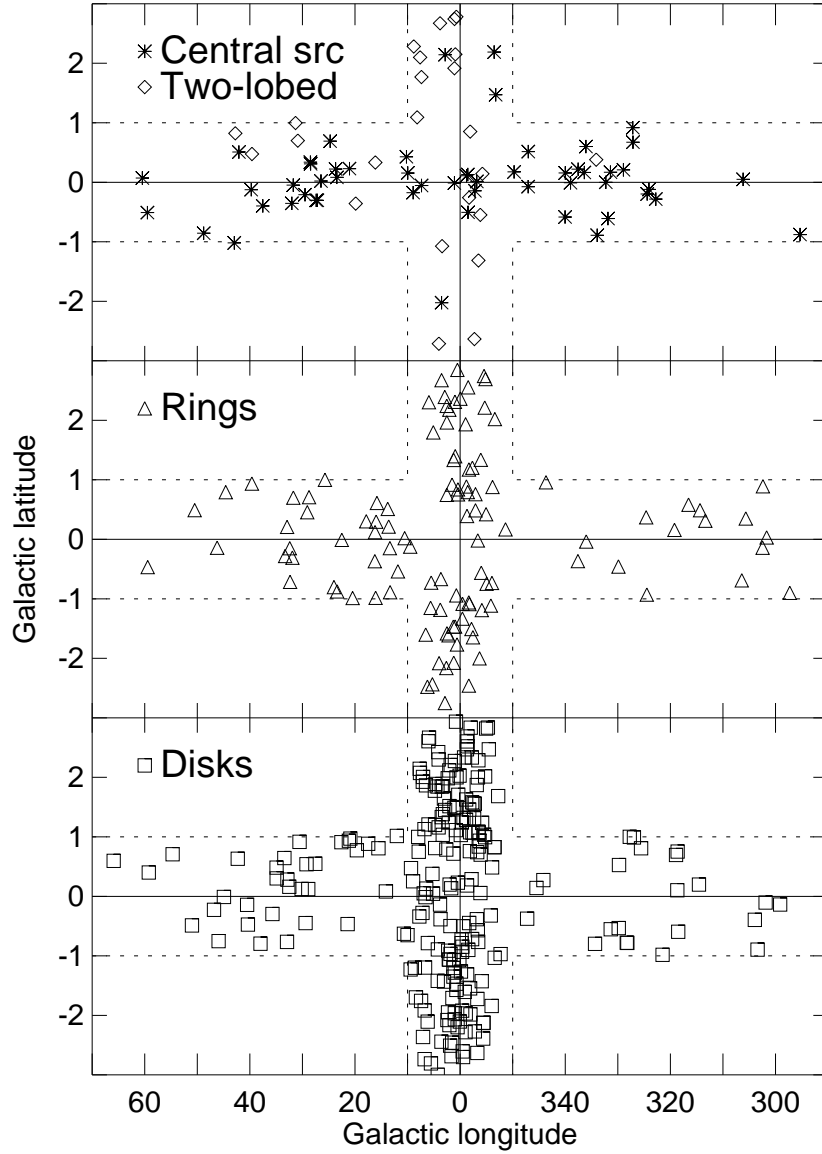


Fig. 8.— Locations of the catalog objects in Galactic coordinates. The dashed lines show the approximate limits of the MIPS GAL survey.

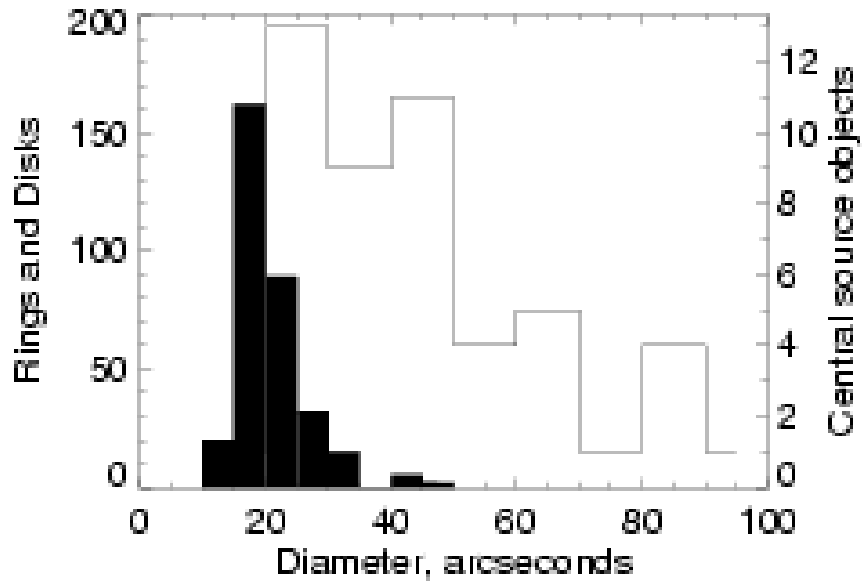


Fig. 9.— Distribution of object diameters for central-source objects (open histogram) and rings and disks combined (filled histogram).

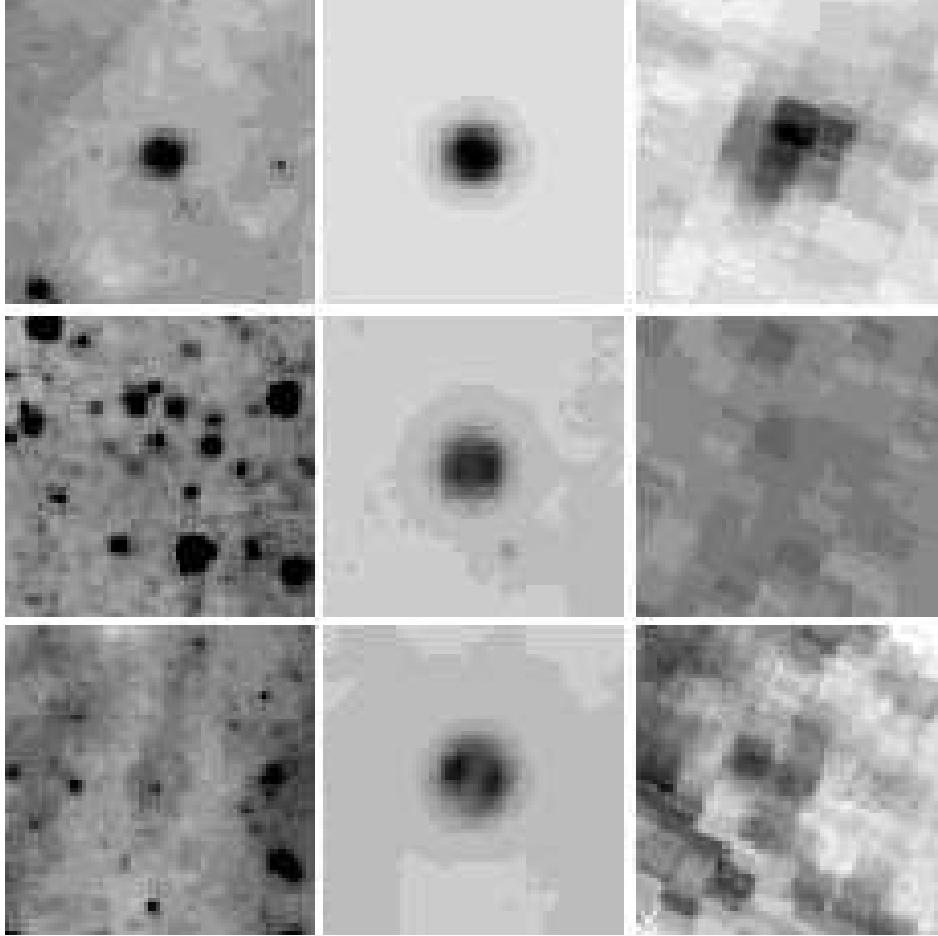


Fig. 10.— Left to right: 8, 24, and 70 μm images. Top: Definite detections at 8 and 70 μm for flat disk MGE030.1503+00.1237. Center: Non-detections, bilaterally symmetric disk MGE002.2728-00.9131. Bottom: Ambiguous detections, bilaterally symmetric disk MGE007.7506-00.3392. Each panel is approximately $1'.3$ across.

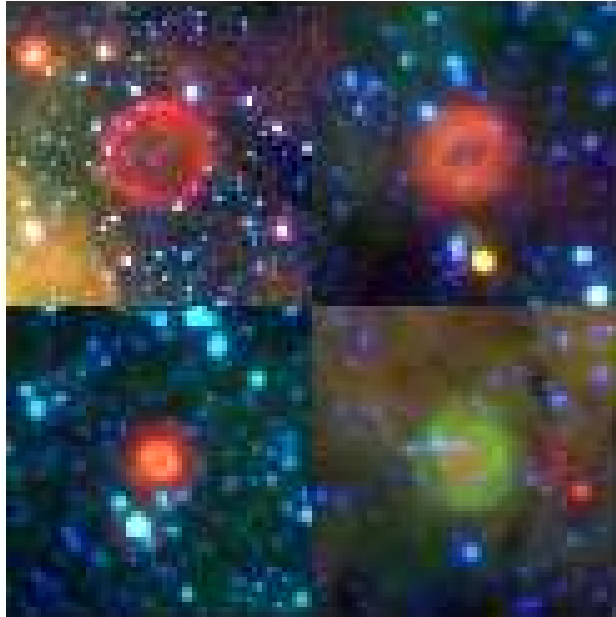


Fig. 11.— Three-color images of four objects. Red: $24\ \mu\text{m}$, green: $8\ \mu\text{m}$, blue: $3.6\ \mu\text{m}$. Upper left: MGE015.8261+00.6109, no $8\ \mu\text{m}$ point source or extended emission. Upper right: MGE029.0781+00.4547, $8\ \mu\text{m}$ emission co-spatial with the $24\ \mu\text{m}$ emission. Lower left: MGE009.3521+00.4736, a thin ring of $8\ \mu\text{m}$ emission interior to the $24\ \mu\text{m}$ emission. Lower right: MGE337.5950-00.3664, the only instance where the $8\ \mu\text{m}$ emission surrounds the $24\ \mu\text{m}$ structure. The image size for MGE015.8261+00.6109 is $4'.2 \times 4'.2$; the other three are $2'.1 \times 2'.1$.

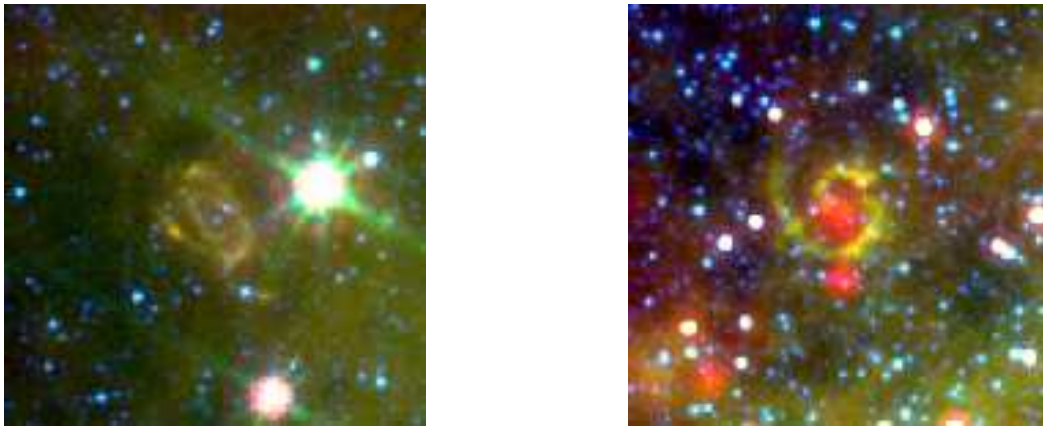


Fig. 12.— Left: Three-color image of MGE314.2378+00.9793. Red: $24\ \mu\text{m}$, green: $8\ \mu\text{m}$, blue: $3.6\ \mu\text{m}$. There is 8 and $24\ \mu\text{m}$ emission from the central source but it is dominated by the $3.6\ \mu\text{m}$ emission with this stretch. The bright star to the right is IRAS 14195-5938. Right: Three-color image of MGE351.2381-00.0145.

Table 1. MIPS GAL disk and ring catalog

Name	J2000 Coordinates		Diam.	F ₂₄	Detection Flags			SIMBAD Associations		
	α (h m s)	δ (° ' ")			(")	(Jy)	8 μ m Point	8 μ m Ext.	70 μ m Ext.	Dist. (")
(1)	(2)	(3)	(4)	(5)	(6)	(7)	(8)	(9)	(10)	(11)
1a: Objects with central sources—regular										
MGE002.8493+02.1430	17 44 05.3	–25 23 16	24	0.04(15)	–	–	?			
MGE003.5216–02.0237	18 01 36.1	–26 55 40	21	0.04(24)	–	–	N			
MGE007.3429–00.0549	18 02 22.3	–22 38 00	32	1.1(80)	Y	Y	–			
MGE008.9460–00.1750	18 06 13.1	–21 17 45	15	0.13(35)	Y	N	?	1.5	HD 313771	*
MGE009.9541+00.1556	18 07 05.2	–20 15 16	28	0.35(18)	Y	?	?			
MGE010.2114+00.4289	18 06 36.2	–19 53 48	40	18.(< 1)	Y	Y ^k	Y	4.3	IRAS 18036–1954	PN?
MGE021.0510+00.2292	18 28 41.5	–10 27 06	45	0.29(99)	Y	N	N			
MGE023.4499+00.0820	18 33 43.4	–08 23 35	25	1.7(34)	Y	N	?			
MGE023.6857+00.2226	18 33 39.5	–08 07 08	44	3.7(29)	Y	N	?			
MGE024.7290+00.6910	18 33 55.3	–06 58 38	50	11.(4)	Y	Y	Y	1.1	V* V481 Sct	LBV
MGE027.1745–00.3041	18 41 59.6	–05 15 41	32	2.6(3)	Y	?	Y			
MGE027.3839–00.3031	18 42 22.5	–05 04 29	38	11.(2)	Y	N	Y	12.2	IRAS 18397–0507	IR
MGE029.5086–00.2090	18 45 55.9	–03 08 30	34	7.0(5)	Y	Y	Y			
MGE031.7516–00.0479	18 49 27.3	–01 04 20	240	8.0(99)	Y	N	?		j	
MGE037.5416–00.3975	19 01 16.6	+03 55 11	42	1.1(19)	Y	?	?	45.5	IRAS 18588+0350 ^e	IR
MGE039.7412–00.1246	19 04 20.9	+06 00 00	46	0.34(39)	Y	N	N			
MGE042.0787+00.5084	19 06 24.5	+08 22 02	21	3.4(< 1)	Y	N	Y	1.6	IRAS 19040+0817	IR
MGE042.9679–01.0183	19 13 32.7	+08 27 04	38	0.12(59)	Y	N	N			
MGE048.7815–00.8565	19 24 03.3	+13 39 50	30	0.14(16)	Y	N	?			
MGE059.4884–00.5093	19 44 42.9	+23 11 34	48	0.18(20)	Y	N	N			
MGE060.4530+00.0712	19 44 37.5	+24 19 06	55	0.84(11)	Y	N	?	7.3	HBHA 2203–01 ^b	Em*
MGE295.3343–00.8786	11 44 17.8	–62 45 21	40	1.6(10)	Y	?	Y	3.5	IRAS 11419–6228	IR
MGE306.1565+00.0494	13 19 33.9	–62 38 46	26	0.99(16)	Y	N	N	1.0	CD–61 3738	*
MGE322.7707–00.2829	15 25 59.7	–57 04 40	22	0.04(20)	Y	Y	Y		i	
MGE324.0739–00.1200	15 33 08.2	–56 12 19	45	1.2(17)	Y	N	?			
MGE324.4138–00.1964	15 35 26.5	–56 04 13	64	0.54(89)	Y	N	Y			
MGE327.1444+00.9168	15 45 59.1	–53 32 33	53	1.4(19)	Y	N	–	10.2	IRAS 15421–5323	IR
MGE328.9301+00.2092	15 58 13.9	–52 57 51	55	2.5(99)	Y	N	?			
MGE331.3971+00.1685	16 10 26.5	–51 21 25	25	1.0(19)	Y	N	?			
MGE332.2843–00.0002	16 15 17.7	–50 52 18	47	106.(–) ^l	Y	N	Y	3.4	IRAS 16115–5044	pA*
MGE333.9204–00.8912	16 26 34.2	–50 21 01	25	9.2(2)	Y	N	Y	22.3	IRAS 16228–5014 ^g	PN?
MGE336.0610+00.6001	16 29 03.8	–47 46 25	33	6.2(2)	Y	Y	Y	16.2	IRAS 16254–4739 ^f	IR
MGE337.5544+00.2198	16 36 42.8	–46 56 21	28	7.5(6)	Y	?	Y			
MGE338.9975–00.0082	16 43 16.2	–46 00 42	60	25.(18)	Y	Y	?	3.7	Wray 16–232	Em*
MGE339.9975+00.1564	16 46 17.3	–45 08 48	24	2.0(24)	Y	N	?			
MGE340.0297–00.5840	16 49 37.7	–45 36 00	85	8.9(89)	Y	N	Y			
MGE347.0305+00.5154	17 08 29.3	–39 25 15	45	0.77(32)	Y	N	Y	4.4	IRAS 17050–3921	IR
MGE347.0516–00.0746	17 11 00.9	–39 45 17	38	5.0(21)	Y	N	?			
MGE353.2347+01.4703	17 22 36.8	–33 49 09	24	0.13(16)	–	–	N			
MGE353.5303+02.1881	17 20 35.1	–33 10 06	225	5.1(27)	–	–	Y	45.0	Wray 15–680 ^a	Em*
MGE356.8235+00.0139	17 37 47.5	–31 37 34	40	1.9(15)	Y	Y	–			
MGE357.1829–00.1434	17 39 19.0	–31 24 22	66	2.9(18)	Y	N	–			
MGE358.5405+00.1299	17 41 35.4	–30 06 38	80	69.(15)	Y	Y	–	1.4	Wray 17–96	LBV
MGE358.7700+00.1088	17 42 14.0	–29 55 36	25	1.2(10)	Y	Y	–			
1b: Objects with central sources—irregular										
MGE001.0860–00.0132	17 48 14.0	–28 00 52	90	61.(28)	Y	?	–	1.1	MWC 272	Em*
MGE026.4700+00.0209	18 39 32.2	–05 44 20	80	86.(2)	Y	Y	Y	1.2	2MASS... ^d	LBV
MGE028.4451+00.3094	18 42 08.2	–03 51 03	80	20.(22)	Y	?	Y			
MGE028.4812+00.3368	18 42 06.3	–03 48 23	240	9.0(99)	Y	?	?			
MGE032.0204–00.3538	18 51 02.1	–00 58 21	66	3.3(55)	?	N	?			
MGE327.1201+00.6731	15 46 52.1	–53 44 58	92	0.50(29)	N	N	?			
MGE331.8690–00.6096	16 16 04.6	–51 35 56	30	42.(–) ^m	Y	?	Y	3.3	IRAS 16122–5128	IR
MGE336.3749+00.1647	16 32 13.9	–47 50 39	70	8.0(30)	?	N	?			
MGE349.7294+00.1747	17 17 59.3	–37 26 09	68	44.(6)	Y	Y	Y	29.8	SNR G349.7+00.2 ^b	SNR
MGE358.5016–00.5048	17 43 59.8	–30 28 39	140	14.(–)	Y	?	–	2.3	[RH184] 10–469 ^b	*
2a: Rings										
MGE000.4176+00.7559	17 43 40.7	–28 11 06	15	0.13(7)	?	N	–			
MGE000.5194+02.8468	17 35 55.6	–26 59 18	22	0.17(5)	–	–	?	1.5	PN G000.5+02.8	PN

Table 1—Continued

Name	J2000 Coordinates		Diam. ($''$)	F ₂₄ (Jy)	Detection Flags			SIMBAD Associations		
	α ($^{\text{h}}$ $^{\text{m}}$ $^{\text{s}}$)	δ ($^{\circ}$ $'$ $''$)			8 μm Point (6)	8 μm Ext. (7)	70 μm Ext. (8)	Dist. ($''$) (9)	Name (10)	Object Type (11)
(1)	(2)	(3)	(4)	(5)	(6)	(7)	(8)	(9)	(10)	(11)
MGE000.7235-00.9420	17 51 00.6	-28 48 10	15	0.01(88)	?	N	N			
MGE000.9363+01.3962	17 42 26.9	-27 24 26	16	0.12(15)	N	N	N			
MGE001.2124-02.0748	17 56 36.2	-28 57 18	18	0.04(13)	N	N	?	3.7	PN G001.2-02.0 ^b	PN?
MGE002.2128-01.6131	17 57 03.9	-27 51 30	18	-27 51 30	?	N	?			
MGE002.5021-01.5808	17 57 35.6	-27 35 31	18	0.08(10)	?	N	N			
MGE002.5220+01.9643	17 44 00.3	-25 45 36	18	0.15(3)	-	-	Y	1.2	PHR J1744-2545	PN?
MGE003.4454-00.6454	17 56 05.2	-26 18 24	63	1.6(< 1)	N	N	?			
MGE003.6547-00.6687	17 56 38.7	-26 08 15	18	0.12(6)	N	N	N			
MGE003.9942-02.0816	18 02 52.2	-26 32 43	18	0.07(17)	-	-	?			
MGE005.5058-00.7281	18 00 57.6	-24 33 47	30	3.3(2)	Y	?	Y	3.2	IRAS 17578-2433	IR
MGE005.6102-01.1516	18 02 48.4	-24 40 54	20	2.3(4)	N	Y	Y	4.3	IRAS 17597-2441	IR
MGE006.2233-02.4777	18 09 13.3	-24 47 36	28	0.05(36)	-	-	N			
MGE010.5569+00.0188	18 08 50.5	-19 47 38	25	0.95(8)	N	N	?	30.0	IRAS 18058-1948	IR
MGE013.3662-00.1483	18 15 09.7	-17 24 40	21	0.44(25)	N	N	?			
MGE013.7676+00.5111	18 13 32.5	-16 44 36	18	0.32(14)	N	N	?			
MGE015.8263+00.6108	18 17 15.4	-14 53 10	45	0.62(22)	N	N	?			
MGE016.1871+00.1202	18 19 45.1	-14 48 02	16	0.05(32)	N	N	N			
MGE023.3894-00.8753	18 37 02.9	-08 53 14	30	0.36(18)	N	N	?			
MGE024.0055-00.8031	18 37 56.0	-08 18 24	21	0.08(35)	N	N	?			
MGE031.9075-00.3087	18 50 40.1	-01 03 09	25	1.4(7)	N	N	?	4.9	PK 031-00 1	PN
MGE039.6131+00.9358	19 00 19.2	+06 22 18	16	0.06(7)	N	N	N			
MGE301.6857+00.0304	12 40 31.4	-62 48 54	17	0.05(7)	N	N	?			
MGE302.3971+00.8908	12 46 53.1	-61 58 34	13	0.01(66)	N	N	-			
MGE306.4142-00.6894	13 22 34.0	-63 21 02	32	2.7(2)	N	Y	Y	0.1	Wray 16-127	PN
MGE316.5509+00.5814	14 41 27.8	-59 20 58	24	0.98(2)	N	N	?			
MGE337.5950-00.3666	16 39 26.1	-47 18 04	24	0.20(41)	Y	Y	?			
MGE354.1474-01.1141	17 35 27.6	-34 29 19	40	0.49(14)	N	N	-			
MGE355.1739+02.6929	17 23 01.6	-31 31 47	24	0.15(7)	-	-	N			
MGE356.0690+01.3365	17 30 39.1	-31 32 32	18	0.04(20)	N	N	N			
MGE357.5633-01.6468	17 46 15.8	-31 52 25	20	0.06(19)	N	N	N			
MGE357.6735+01.2030	17 35 15.0	-30 16 11	21	0.15(7)	?	N	-			
MGE358.2249-01.0885	17 45 38.4	-31 01 06	15	0.04(26)	N	N	N			
MGE358.3271+01.1733	17 36 59.4	-29 44 07	26	0.19(6)	N	N	N			
MGE358.3478-01.0603	17 45 49.6	-30 53 55	22	0.03(38)	N	N	N			
MGE358.4694+02.5544	17 32 01.1	-28 52 05	24	0.05(14)	-	-	N			
MGE358.6905+00.3921	17 40 55.8	-29 50 40	15	0.08(22)	N	N	-	4.5	[DVC98] 6	Rad
2b: Rings—irregular										
MGE000.4100+00.8386	17 43 20.5	-28 08 53	18	0.21(12)	N	N	?			
MGE000.5910-01.7683	17 53 57.5	-29 20 14	25	0.25(7)	?	N	N	4.7	JaSt 96	PN
MGE000.9516-01.4656	17 53 35.9	-28 52 23	18	0.12(14)	N	N	?	4.2	JaSt2 13	PN
MGE000.9899+02.3115	17 39 05.1	-26 52 39	21	0.27(4)	-	-	?			
MGE001.2343+01.3341	17 43 23.4	-27 11 12	25	0.13(11)	?	N	N	5.3	JaSt 45	PN
MGE001.2920-01.4680	17 54 23.6	-28 34 51	15	0.03(14)	N	N	N	0.4	JaSt2 15	PN
MGE001.5280+00.9171	17 45 40.7	-27 09 15	18	0.20(7)	N	N	?			
MGE002.0644+02.1789	17 42 07.5	-26 02 12	30	0.05(33)	-	-	?			
MGE002.5276+00.7462	17 48 39.2	-26 23 16	18	0.18(9)	?	N	-			
MGE002.5424+02.2426	17 43 00.0	-25 35 49	25	0.05(18)	-	-	?			
MGE002.6193-02.1625	18 00 08.1	-27 46 48	23	0.02(51)	-	-	N			
MGE002.9176+02.3920	17 43 18.5	-25 11 57	25	0.01(42)	-	-	N			
MGE003.5282+02.6745	17 43 39.3	-24 31 54	50	0.69(3)	-	-	Y	1.6	PN G003.5+02.7 ^b	PN
MGE003.7724-01.1833	17 58 53.6	-26 17 35	28	0.30(8)	N	N	?			
MGE005.2835-02.4370	18 07 03.3	-25 35 43	25	0.46(4)	-	-	?	1.2	PHR J1807-2535	PN
MGE005.9347+02.3035	17 50 28.1	-22 39 57	30	0.05(15)	-	-	N			
MGE006.5449-01.6013	18 06 32.4	-24 05 14	34	0.29(33)	-	-	N			
MGE009.4947-00.1225	18 07 10.1	-20 47 28	20	0.15(15)	N	N	N			
MGE011.8322-00.5388	18 13 31.1	-18 56 42	26	0.47(14)	Y	N	Y			
MGE013.3211-00.8896	18 17 48.5	-17 48 12	18	0.32(6)	N	Y	N			
MGE015.9774+00.2955	18 18 42.2	-14 54 09	18	0.18(51)	?	N	?			
MGE016.0749-00.9833	18 23 34.1	-15 25 07	25	0.13(42)	N	N	-			
MGE016.2280-00.3680	18 21 36.9	-14 59 41	18	0.30(35)	?	N	?	3.5	GPSR5 16.228-0.369	Rad
MGE017.8638+00.3028	18 22 20.6	-13 14 08	20	0.15(23)	?	N	?			

Table 1—Continued

Name	J2000 Coordinates		Diam. (")	F ₂₄ (Jy)	Detection Flags			SIMBAD Associations		
	α (h m s)	δ (° ' ")			8 μ m Point (6)	8 μ m Ext. (7)	70 μ m Ext. (8)	Dist. (") (9)	Name (10)	Object Type (11)
(1)	(2)	(3)	(4)	(5)	(6)	(7)	(8)	(9)	(10)	(11)
MGE020.4513-00.9867	18 31 57.1	-11 32 46	32	0.35(14)	N	N	-			
MGE025.7137+01.0007	18 34 38.4	-05 57 38	17	0.04(61)	N	N	?			
MGE028.7440+00.7076	18 41 16.0	-03 24 11	23	0.25(10)	N	N	?			
MGE031.7290+00.6993	18 46 45.2	-00 45 06	44	1.2(8)	?	Y ^k	Y	12.7	IRAS 18441-0048	IR
MGE032.3506-00.7153	18 52 55.4	-00 50 37	23	0.11(34)	N	N	?			
MGE032.4006-00.1507	18 51 00.3	-00 32 30	33	0.69(7)	Y	N	?			
MGE046.2242-00.1416	19 16 32.6	+11 44 30	25	0.11(23)	N	N	N			
MGE050.5016+00.4896	19 22 30.4	+15 48 56	28	0.33(5)	?	N	?			
MGE059.4354-00.4662	19 44 26.3	+23 10 06	25	0.07(21)	N	N	N			
MGE297.2836-00.8995	12 00 58.8	-63 13 00	23	0.06(18)	?	N	N	12.3	HD 104375	*
MGE302.4617-00.1412	12 47 17.6	-63 00 33	20	0.15(23)	N	N	?			
MGE305.6516+00.3494	13 14 56.9	-62 23 53	19	0.59(33)	Y	?	N			
MGE313.3544+00.3123	14 18 27.6	-60 47 11	24	0.81(3)	N	Y	?	0.2	PN G313.3+00.3 ^b	PN
MGE314.3603+00.4880	14 25 39.2	-60 16 35	20	0.08(29)	?	Y	?			
MGE319.2193+00.1581	15 01 27.5	-58 32 26	26	1.3(4)	N	N	?			
MGE324.4811-00.9290	15 38 56.9	-56 37 21	18	0.03(99)	N	N	?			
MGE324.6051+00.3692	15 34 12.4	-55 29 56	25	0.21(7)	?	Y	Y			
MGE329.8780-00.4579	16 05 52.6	-52 50 35	40	0.09(99)	N	N	N			
MGE336.0114-00.0381	16 31 37.9	-48 14 54	28	4.3(8)	Y	N	Y	28.4	IRAS 16278-4808 ^h	IR
MGE343.6641+00.9584	16 55 46.9	-41 48 42	21	0.13(22)	?	N	N			
MGE351.3662+00.1671	17 22 41.4	-36 05 50	18	0.11(13)	?	N	N			
MGE353.3934+02.0206	17 20 52.2	-33 22 34	18	0.17(6)	-	-	N			
MGE353.8415+00.8789	17 26 36.4	-33 39 00	15	0.13(14)	N	N	?			
MGE353.9398-00.7336	17 33 21.8	-34 27 24	24	0.47(4)	N	N	-			
MGE354.9589-00.7468	17 36 04.8	-33 36 26	15	0.15(11)	N	N	N			
MGE355.0606+00.4209	17 31 39.4	-32 53 15	15	0.27(4)	?	N	?			
MGE355.3208+02.2134	17 25 16.6	-31 40 40	23	0.05(23)	-	-	-			
MGE355.4464+02.7440	17 23 32.9	-31 16 34	20	0.01(78)	-	-	N			
MGE355.8710-01.1891	17 40 12.3	-33 04 24	24	0.08(18)	N	N	N			
MGE355.9808-00.5628	17 37 57.6	-32 38 48	24	0.09(25)	?	N	-			
MGE356.3082-02.0001	17 44 35.8	-33 07 43	25	0.09(10)	-	-	N			
MGE356.6350-00.0191	17 37 26.8	-31 48 10	18	0.06(13)	Y	Y	-			
MGE357.0783+00.4869	17 36 33.7	-31 09 26	15	0.11(23)	N	N	-			
MGE357.0801+00.7581	17 35 30.0	-31 00 34	15	0.02(37)	?	N	N			
MGE357.8415-01.5069	17 46 22.8	-31 33 48	28	0.04(35)	?	N	N			
MGE358.3425-02.4585	17 51 25.3	-31 37 24	21	0.06(10)	-	-	N			
MGE358.5502+00.7938	17 39 01.0	-29 44 59	18	0.21(9)	N	N	?			
MGE358.8068+00.8872	17 39 17.0	-29 28 59	16	0.22(6)	N	N	?			
MGE358.9577+01.9334	17 35 36.5	-28 47 42	24	0.16(6)	?	N	N			
MGE359.5381-01.0838	17 48 46.6	-29 53 34	23	0.03(15)	?	N	?			
MGE359.5605-01.3330	17 49 49.0	-30 00 06	25	0.18(7)	?	?	?			
MGE359.9600+02.3633	17 36 24.6	-27 43 10	29	0.03(19)	-	-	?			
2c: Rings—bilaterally symmetric										
MGE002.8866-02.7510	18 03 02.8	-27 50 17	22	0.05(15)	-	-	?			
MGE005.1020+01.7969	17 50 30.6	-23 38 24	18	0.16(7)	-	-	N			
MGE013.5944+00.2139	18 14 17.1	-17 02 15	24	0.39(11)	N	N	N			
MGE022.5082-00.0086	18 32 17.3	-09 16 13	19	0.17(31)	?	N	N			
MGE029.0784+00.4545	18 42 46.8	-03 13 17	28	2.1(11)	Y	Y	Y	2.0	PN A55 36	PN
MGE032.9141+00.2088	18 50 39.7	+00 04 46	30	2.2(8)	Y	N	Y	9.9	IRAS 18481+0001	IR
MGE033.2929-00.2805	18 53 05.7	+00 11 36	25	0.28(19)	Y	N	?			
MGE044.5870+00.7927	19 10 04.3	+10 43 28	27	0.16(11)	N	N	N			
3a: Disks—flat										
MGE000.1134-00.0975	17 46 16.2	-28 53 24	16	1.2(13)	?	N	?			
MGE000.6925-01.4687	17 53 00.6	-29 05 52	18	0.08(7)	N	N	N	9.6	JaSt 88	PN
MGE000.7067-01.5718	17 53 27.0	-29 08 17	15	0.30(3)	?	N	?	1.0	JaSt2 11	PN
MGE001.0178-01.9642	17 55 43.1	-29 04 04	28	1.4(2)	?	Y	Y	4.5	PN K 6-35 ^b	PN
MGE001.0930+01.4875	17 42 28.2	-27 13 34	23	0.11(9)	N	N	N	4.1	JaSt2 4	PN
MGE001.7985+02.2079	17 41 23.5	-26 14 50	20	0.03(11)	-	-	N			
MGE001.8248-00.9674	17 53 39.5	-27 52 05	16	0.12(8)	N	N	?			

Table 1—Continued

Name	J2000 Coordinates		Diam. ($''$)	F ₂₄ (Jy)	Detection Flags			SIMBAD Associations		
	α (h m s)	δ ($^{\circ}$ ' $''$)			8 μ m Point (6)	8 μ m Ext. (7)	70 μ m Ext. (8)	Dist. ($''$) (9)	Name (10)	Object Type (11)
(1)	(2)	(3)	(4)	(5)	(6)	(7)	(8)	(9)	(10)	(11)
MGE001.8960-02.5094	17 59 52.6	-28 34 47	16	0.09(7)	–	–	N			
MGE002.0411-02.1635	17 58 50.3	-28 16 55	20	0.06(12)	–	–	?	1.2	PN G001.9-02.5	PN?
MGE002.1530-01.0607	17 54 46.3	-27 37 56	16	0.10(10)	?	N	N			
MGE002.3535+01.9852	17 43 32.1	-25 53 33	22	0.04(19)	–	–	N			
MGE002.6242+00.7861	17 48 43.4	-26 17 04	12	0.02(17)	N	N	–			
MGE003.5004+01.8442	17 46 42.8	-24 59 16	18	0.07(17)	–	–	N			
MGE005.5423-02.8069	18 09 02.7	-25 32 53	20	0.29(3)	–	–	Y			
MGE005.9143+02.6666	17 49 04.3	-22 29 50	24	0.02(33)	–	–	N			
MGE006.0270+02.6063	17 49 32.8	-22 25 53	18	0.03(15)	–	–	?			
MGE006.4993+01.8661	17 53 20.6	-22 24 10	18	0.05(18)	–	–	N			
MGE006.7488-01.9183	18 08 11.2	-24 03 47	18	0.27(14)	–	–	?			
MGE007.6440+02.0742	17 55 03.6	-21 18 38	16	0.12(4)	–	–	N	0.2	PHR J1755-2118	PN
MGE009.4257-01.2294	18 11 10.6	-21 23 15	20	1.6(2)	–	–	–	1.1	PN G009.4-01.2 ^b	PN
MGE010.6846-00.6280	18 11 30.8	-19 59 41	15	0.40(9)	N	N	?			
MGE014.1176+00.0816	18 15 48.9	-16 38 27	15	0.20(46)	?	N	N			
MGE015.5409+00.8084	18 15 58.5	-15 02 36	20	0.06(29)	N	N	?			
MGE017.4818+00.8837	18 19 29.9	-13 17 56	27	0.74(11)	N	N	?			
MGE019.6492+00.7740	18 24 04.0	-11 26 16	18	0.29(4)	?	?	Y			
MGE021.1662+00.9358	18 26 22.1	-10 01 15	20	0.02(51)	N	N	?			
MGE028.8843+00.1226	18 43 36.5	-03 32 44	16	0.09(36)	N	N	N			
MGE029.4034-00.4496	18 46 35.9	-03 20 43	16	0.08(27)	N	N	?			
MGE030.1503+00.1237	18 45 55.2	-02 25 08	26	9.3(< 1)	Y	Y ^k	Y	2.2	IRAS 18433-0228	IR
MGE030.5495+00.9160	18 43 49.7	-01 42 07	15	0.26(31)	N	N	?			
MGE033.4364+00.6435	18 50 04.0	+00 44 33	21	0.03(54)	N	N	N			
MGE040.5176-00.1423	19 05 50.8	+06 40 54	18	0.17(20)	?	N	?			
MGE051.0214-00.4885	19 27 06.7	+15 48 35	18	0.46(3)	N	Y	Y			
MGE303.4121-00.8953	12 55 46.9	-63 45 47	18	0.12(36)	N	N	?			
MGE314.5620+00.1984	14 28 01.2	-60 28 26	16	0.36(3)	N	N	N			
MGE318.6864+00.1018	14 58 02.9	-58 50 31	21	0.23(9)	N	N	?			
MGE327.7248+01.0008	15 48 41.6	-53 07 04	21	0.39(8)	N	Y	–			
MGE328.2972-00.7801	15 59 18.9	-54 07 39	24	0.09(17)	N	N	?			
MGE329.7690+00.5262	16 01 03.7	-52 10 37	30	0.27(30)	?	N	?			
MGE329.8273-00.5329	16 05 57.6	-52 55 58	16	0.53(2)	N	N	Y			
MGE331.3471-00.5530	16 13 22.9	-51 55 05	15	0.29(23)	Y	N	?			
MGE347.2495-00.3759	17 12 53.3	-39 46 22	16	0.24(11)	N	N	?			
MGE352.7640+01.6844	17 20 28.4	-34 05 05	15	0.06(13)	–	–	N			
MGE354.0020-01.8419	17 38 04.1	-35 00 08	18	0.08(8)	–	–	–			
MGE354.1575-00.3221	17 32 16.1	-34 03 00	18	0.05(22)	N	N	–			
MGE354.7174+02.8360	17 21 15.6	-31 49 28	18	0.07(13)	–	–	?			
MGE355.5334-02.1243	17 43 09.6	-33 51 12	22	0.05(14)	–	–	?			
MGE355.6162-02.3903	17 44 27.7	-33 55 19	33	0.11(26)	–	–	N	3.8	PHR J1744-3355	PN
MGE356.2849+00.9344	17 32 47.2	-31 34 54	18	0.43(11)	?	N	–			
MGE356.7274-02.6316	17 48 12.7	-33 05 52	18	0.01(39)	–	–	N			
MGE357.2028-02.2696	17 47 54.0	-32 30 15	18	0.08(16)	–	–	N			
MGE357.6548+01.0694	17 35 43.4	-30 21 28	18	0.52(10)	N	N	Y	2.2	PK 357+01 3	PN
MGE358.7080+02.4704	17 32 55.9	-28 42 50	15	0.03(15)	–	–	N			
MGE358.7131+02.6027	17 32 26.3	-28 38 15	18	0.03(12)	–	–	N			
MGE358.8655+01.2862	17 37 52.7	-29 13 13	15	0.15(6)	N	N	N			
MGE359.2412+02.3353	17 34 45.8	-28 20 22	24	0.09(13)	–	–	N			
MGE359.7169-00.7867	17 48 01.8	-29 35 11	16	0.17(30)	?	?	?			
MGE359.7280-00.7201	17 47 47.6	-29 32 33	20	0.09(30)	N	N	?			
MGE359.8429-01.2646	17 50 12.8	-29 43 27	20	0.13(10)	?	N	?			
3b: Disks—peaked										
MGE000.1495-01.0708	17 50 10.3	-29 21 42	14	0.15(7)	Y	N	N			
MGE000.4284+00.2292	17 45 44.7	-28 27 04	14	0.08(38)	N	N	–			
MGE000.8076+01.1132	17 43 13.7	-27 39 56	14	0.03(18)	N	N	?			
MGE001.6982+00.1362	17 49 04.9	-27 24 47	18	0.08(16)	N	N	–			
MGE002.0287+01.5161	17 44 33.5	-26 24 53	14	0.04(11)	N	N	?	7.8	JaSt 50	PN
MGE003.0836+01.6435	17 46 31.0	-25 26 53	13	0.13(5)	–	–	?			
MGE003.2861+01.3814	17 47 58.5	-25 24 38	16	0.36(2)	N	N	Y			
MGE003.7287-00.3847	17 55 43.1	-25 55 51	12	0.02(22)	N	N	–			

Table 1—Continued

Name	J2000 Coordinates		Diam.	F ₂₄	Detection Flags			SIMBAD Associations		
	α (h m s)	δ ($^{\circ}$ ' ")			(")	(Jy)	8 μ m Point (6)	8 μ m Ext. (7)	70 μ m Ext. (8)	Dist. (") (9)
(1)	(2)	(3)	(4)	(5)	(6)	(7)	(8)	(9)	(10)	(11)
MGE004.3111+01.8455	17 48 33.1	-24 17 36	18	0.33(4)	–	–	Y	0.2	PHR J1748-2417	PN
MGE004.7474+00.8115	17 53 26.0	-24 26 49	13	0.03(13)	N	N	–			
MGE006.1745-02.1048	18 07 40.9	-24 39 20	16	0.11(8)	–	–	?	2.5	PN G006.1-02.1	PN
MGE006.4395+00.1299	17 59 43.8	-23 19 35	16	1.2(2)	N	Y	?			
MGE006.9367+00.0497	18 01 06.4	-22 56 05	20	0.10(35)	N	N	N			
MGE007.1627-00.2781	18 02 49.7	-22 54 01	11	0.02(71)	?	N	–			
MGE029.2228+00.5392	18 42 44.6	-03 03 15	16	0.17(16)	N	N	N			
MGE032.4982+00.1615	18 50 04.3	-00 18 44	16	0.60(3)	Y	Y	?	2.3	G032.498+0.161 ⁿ	Rad
MGE032.8593+00.2806	18 50 18.4	+00 03 48	15	0.44(6)	N	N	?	1.4	G032.859+0.280 ⁿ	Rad
MGE040.3704-00.4750	19 06 45.8	+06 23 53	27	1.1(4)	N	Y ^k	Y	2.1	PN A55 41	PN
MGE044.9328-00.0101	19 13 37.2	+10 39 34	21	0.07(11)	N	N	?	4.4	PN G044.9+00.0	PN
MGE301.8797-00.1036	12 42 10.7	-62 57 23	16	0.03(20)	N	N	N			
MGE352.3117-00.9711	17 29 58.3	-35 56 56	18	0.37(9)	N	N	Y			
MGE353.4200-01.0326	17 33 12.4	-35 03 20	15	0.21(6)	?	N	–			
MGE353.4568+00.8258	17 25 47.0	-33 59 55	16	0.17(18)	N	N	–			
MGE354.5377+02.4713	17 22 11.7	-32 10 45	27	0.67(2)	–	–	Y	0.5	PHR J1722-3210 ^b	PN
MGE355.0574+02.8195	17 22 13.7	-31 33 15	16	0.04(14)	–	–	?			
MGE355.2534+02.0154	17 25 52.3	-31 50 40	15	0.13(58)	–	–	N			
MGE356.5561-00.7652	17 40 13.6	-32 16 04	14	0.15(20)	N	N	–			
MGE356.6214+01.9982	17 29 29.5	-30 43 01	16	0.10(8)	–	–	N			
MGE356.8155-00.3843	17 39 21.3	-31 50 44	15	0.72(4)	?	N	–	5.0	GPSR5 356.816-0.385	Rad
MGE357.2013+01.5550	17 32 41.4	-30 28 31	16	0.05(9)	?	N	N			
MGE357.7075-00.7184	17 42 54.1	-31 15 56	14	0.20(16)	N	N	–			
MGE357.7077+01.5812	17 33 51.9	-30 02 10	16	0.07(12)	N	N	N			
MGE357.7758+02.3326	17 31 07.9	-29 34 10	16	0.04(24)	–	–	N			
MGE359.3684+01.3182	17 38 59.0	-28 46 41	16	0.24(4)	N	N	N	5.1	JaSt 12	PN
MGE359.6760+01.2410	17 40 01.6	-28 33 32	15	0.22(5)	?	N	?			
3c: Disks—bilaterally symmetric										
MGE000.0689-02.1037	17 54 04.5	-29 57 25	18	0.25(6)	Y	N	?			
MGE000.1107+02.0286	17 38 03.2	-27 46 18	18	0.47(2)	?	?	Y	4.3	PHR J1738-2746	PN
MGE000.6713+01.4999	17 41 25.2	-27 34 40	21	0.15(5)	N	N	?			
MGE001.0040-01.2822	17 52 59.9	-28 44 06	18	0.25(5)	N	N	N	11.5	JaSt 87	PN
MGE001.0098-02.0666	17 56 06.3	-29 07 34	18	0.08(15)	N	N	?			
MGE002.0599-01.0642	17 54 34.4	-27 42 51	27	0.95(4)	?	N	?			
MGE002.2728-00.9131	17 54 28.2	-27 27 15	18	0.35(5)	N	N	N			
MGE003.0631-01.4329	17 58 16.7	-27 01 56	15	0.01(43)	N	N	N			
MGE003.3094+01.0342	17 49 20.8	-25 34 10	15	0.03(23)	N	N	N			
MGE003.5533-02.4421	18 03 18.4	-27 06 22	30	6.0(2)	–	–	–	1.0	IC 4673	PN
MGE003.8301-00.1385	17 55 00.0	-25 43 09	20	7.5(2)	Y	Y	–	19.6	IRAS 17519-2542 ^j	IR
MGE006.1437-00.7853	18 02 33.7	-24 02 13	18	0.06(35)	N	N	–			
MGE006.5850-00.0135	18 00 35.2	-23 16 17	12	0.02(61)	N	N	?			
MGE006.7840+01.1298	17 56 43.0	-22 31 42	17	0.01(62)	?	N	N			
MGE007.0582-02.3635	18 10 32.9	-24 00 27	18	0.20(14)	–	–	?			
MGE007.7506-00.3392	18 04 18.8	-22 25 07	18	0.47(6)	Y	?	?			
MGE007.8745+00.7500	18 00 29.3	-21 46 23	18	0.14(9)	Y	N	?			
MGE008.5984-01.1993	18 09 20.7	-22 05 50	18	0.05(17)	–	–	N			
MGE032.9266-00.7652	18 54 09.1	-00 21 13	18	0.02(22)	N	N	N			
MGE034.8961+00.3018	18 53 56.8	+01 53 08	21	0.27(12)	N	N	N			
MGE037.9742-00.7954	19 03 29.4	+04 07 20	20	0.12(14)	?	N	?			
MGE045.9426-00.7527	19 18 12.7	+11 12 26	28	0.06(24)	?	N	?			
MGE321.4940-00.9818	15 20 51.9	-58 21 43	18	0.08(10)	Y	?	N			
MGE325.5783+00.8074	15 37 55.2	-54 34 25	15	0.06(7)	N	N	N			
MGE326.9346+00.9894	15 44 34.1	-53 36 48	14	0.06(31)	N	N	–			
MGE344.1648+00.2733	17 00 20.0	-41 50 43	24	0.99(3)	N	Y	Y			
MGE345.4797+00.1407	17 05 10.4	-40 53 06	21	12.(4)	N	Y	Y	2.8	IC 4637	PN
MGE356.4594+01.0730	17 32 41.3	-31 21 35	18	0.08(16)	?	N	–			
MGE356.5247+02.2864	17 28 07.6	-30 38 17	20	0.45(6)	–	–	Y	2.4	PHR J1728-3038	PN
MGE356.8316+01.8709	17 30 31.4	-30 36 42	17	0.07(82)	–	–	N			
MGE357.3340+01.3123	17 33 58.3	-30 29 45	21	0.20(6)	N	?	N	0.4	PHR J1733-3029	PN
MGE357.4403+01.5640	17 33 15.5	-30 16 12	20	0.04(23)	?	N	N			
MGE358.0310-01.9836	17 48 45.4	-31 38 51	18	0.10(26)	Y	N	N			

Table 1—Continued

Name	J2000 Coordinates		Diam.	F ₂₄	Detection Flags			SIMBAD Associations		
	α (h m s)	δ ($^{\circ}$ ' ")			(")	(Jy)	8 μ m Point	8 μ m Ext.	70 μ m Ext.	Dist. (")
(1)	(2)	(3)	(4)	(5)	(6)	(7)	(8)	(9)	(10)	(11)
MGE358.4433-00.8992	17 45 25.0	-30 44 00	15	0.07(20)	?	?	N			
MGE358.6888+00.1824	17 41 44.8	-29 57 25	10	0.06(99)	N	N	-			
MGE359.6256-00.9322	17 48 23.2	-29 44 23	26	0.07(19)	?	N	?			
3d: Disks—oblong										
MGE000.3521+01.7064	17 39 52.0	-27 44 20	16	0.18(3)	N	N	Y	13.4	JaSt 21	PN
MGE001.2693+00.7174	17 45 50.4	-27 28 44	16	0.44(2)	Y	N	?			
MGE001.5182-02.4587	17 58 49.2	-28 52 55	16	0.03(10)	-	-	?	0.6	PN G001.5-02.4	PN
MGE001.8562-00.4996	17 51 54.6	-27 36 11	12	0.07(11)	N	N	-			
MGE002.1604+01.2401	17 45 55.0	-26 26 46	16	0.28(3)	N	N	Y	3.8	PN G002.1+01.2	PN?
MGE003.2610+01.8522	17 46 08.1	-25 11 17	15	0.07(11)	-	-	?			
MGE006.0169+01.2081	17 54 44.8	-23 09 06	18	0.21(7)	-	-	Y	1.2	PHR J1754-2309	PN?
MGE007.0999+01.9268	17 54 25.7	-21 51 15	20	0.06(15)	-	-	?			
MGE007.4345-01.7575	18 09 01.3	-23 23 08	16	0.10(13)	-	-	N			
MGE007.9853+00.9983	17 59 47.8	-21 33 13	16	0.28(6)	N	N	Y			
MGE008.9409+00.2532	18 04 36.3	-21 05 26	18	0.49(5)	?	Y	?	1.6	G008.94097+0.25373 ^o	Rad
MGE009.3523+00.4733	18 04 38.9	-20 37 27	28	2.5(2)	N	Y	Y	0.2	PN PBOZ 33	PN?
MGE299.1183-00.1370	12 18 00.9	-62 45 40	18	0.04(21)	N	N	N	1.0	PHR J1218-6245	PN?
MGE318.9322+00.6959	14 57 35.5	-58 12 06	28	1.8(2)	N	Y	Y	4.0	PHR J1457-5818 ^b	PN
MGE358.2714-00.4486	17 43 12.8	-30 38 38	16	0.45(12)	N	N	-			
MGE358.8567+01.6271	17 36 32.4	-29 02 42	20	0.14(5)	N	N	N			
MGE358.9299-01.9684	17 50 51.1	-30 52 07	15	0.06(9)	N	N	N			
MGE359.5784-00.8461	17 47 56.1	-29 44 08	26	0.23(14)	N	Y	?			
3e: Disks—irregular										
MGE000.4900-02.1986	17 55 25.9	-29 38 29	25	0.09(55)	-	-	Y	6.8	OGLEII... ^c	EB*
MGE000.6829+01.9996	17 39 32.3	-27 18 11	15	0.00(40)	N	N	N			
MGE000.7880+02.9357	17 36 14.2	-26 42 51	20	0.03(28)	-	-	N			
MGE000.9934+02.2747	17 39 13.9	-26 53 39	13	0.01(29)	-	-	N			
MGE001.1947-01.0735	17 52 37.3	-28 27 53	20	0.09(21)	N	N	N			
MGE001.2760-01.3496	17 53 53.5	-28 32 05	24	0.09(18)	N	N	N			
MGE001.2846-01.2034	17 53 20.3	-28 27 11	21	0.32(5)	N	N	N	6.1	JaSt 92	PN
MGE001.4688-01.7089	17 55 44.8	-28 32 59	20	0.04(21)	?	N	?			
MGE001.6301-02.6875	17 59 58.9	-28 53 55	18	0.12(15)	-	-	?	26.6	PHR J1759-2853 ^b	PN
MGE001.9965+00.1976	17 49 32.1	-27 07 32	12	0.03(85)	N	N	-			
MGE002.0557+02.1161	17 42 20.6	-26 04 38	20	0.01(50)	N	N	N			
MGE002.3014-01.9492	17 58 35.0	-27 56 59	18	0.07(7)	N	N	N	3.6	PHR J1758-2756	PN
MGE002.4094-02.0786	17 59 20.1	-27 55 14	13	0.00(33)	?	N	?			
MGE002.8530+01.4514	17 46 42.9	-25 44 41	18	0.07(9)	?	N	?			
MGE003.5014+01.3314	17 48 39.3	-25 15 07	20	0.03(18)	?	N	?			
MGE004.0775+02.2998	17 46 18.9	-24 15 30	24	0.05(22)	-	-	N			
MGE004.0816+01.1591	17 50 37.4	-24 50 34	26	0.50(6)	?	N	?			
MGE004.1668+02.4238	17 46 03.2	-24 07 04	24	0.08(15)	-	-	N			
MGE004.2374-00.8916	17 58 48.0	-25 44 41	18	0.18(5)	?	N	N			
MGE004.2573-02.9981	18 07 01.4	-26 45 49	42	0.39(10)	-	-	?			
MGE004.2590-01.4204	18 00 53.3	-25 59 20	23	0.06(16)	?	N	N			
MGE004.6913+01.8888	17 49 14.7	-23 56 43	21	0.02(28)	-	-	N	2.3	PN G004.6+01.8	PN
MGE004.7784+01.2007	17 52 01.8	-24 13 21	23	0.07(13)	N	N	N			
MGE004.8004+01.7757	17 49 54.9	-23 54 35	25	0.10(9)	-	-	N			
MGE005.1516+00.0444	17 57 14.4	-24 29 06	20	0.24(16)	N	N	-			
MGE005.2641+00.3775	17 56 13.4	-24 13 13	16	1.1(2)	?	Y	-	2.7	G005.264+0.377 ⁿ	Rad
MGE006.6637-01.1965	18 05 14.8	-23 47 09	27	0.05(23)	-	-	N			
MGE006.7691-02.7365	18 11 22.5	-24 26 24	24	0.21(5)	-	-	?			
MGE007.0571+02.0063	17 54 02.4	-21 51 04	15	0.01(31)	-	-	N			
MGE007.6985+02.1443	17 54 55.1	-21 13 41	24	0.02(33)	-	-	N			
MGE008.4067-01.6982	18 10 50.0	-22 30 21	16	0.12(4)	-	-	N	16.0	G008.405-1.694 ⁿ	Rad
MGE010.0155-00.6520	18 10 13.7	-20 35 33	21	0.06(24)	N	N	N			
MGE012.0367+01.0149	18 08 11.6	-18 01 01	32	0.09(40)	N	N	N			
MGE020.8749+00.9698	18 25 41.6	-10 15 46	18	0.04(21)	N	N	N			
MGE021.4030-00.4666	18 31 51.8	-10 27 43	21	0.09(18)	?	N	?			
MGE022.5964+00.9098	18 29 09.4	-08 46 01	18	0.06(25)	N	N	N			

Table 1—Continued

Name	J2000 Coordinates		Diam. ($''$)	F ₂₄ (Jy)	Detection Flags			SIMBAD Associations		
	α (h m s)	δ ($^{\circ}$ ' $''$)			8 μ m Point (6)	8 μ m Ext. (7)	70 μ m Ext. (8)	Dist. ($''$) (9)	Name (10)	Object Type (11)
(1)	(2)	(3)	(4)	(5)	(6)	(7)	(8)	(9)	(10)	(11)
MGE027.5373+00.5473	18 39 37.3	-04 32 57	15	0.07(23)	N	N	N			
MGE034.9249+00.4834	18 53 21.1	+01 59 39	15	0.09(38)	N	N	?			
MGE035.7017-00.2975	18 57 33.1	+02 19 45	19	0.06(17)	N	Y	Y			
MGE042.3030+00.6323	19 06 22.9	+08 37 24	28	0.04(31)	N	Y	?			
MGE046.8232-00.2257	19 17 59.4	+12 13 55	18	0.03(36)	N	N	?			
MGE054.6957+00.7074	19 30 04.6	+19 36 31	18	0.08(13)	N	Y	Y			
MGE059.2301+00.4005	19 40 43.1	+23 25 15	21	0.07(12)	N	N	N			
MGE065.9141+00.5966	19 55 02.4	+29 17 20	33	1.1(4)	-	-	Y	0.8	NGC 6842	PN
MGE303.9339-00.3946	13 00 20.6	-63 14 56	25	0.10(20)	?	Y	Y			
MGE318.5117-00.5950	14 59 23.8	-59 32 21	28	0.29(10)	?	N	?			
MGE318.6228+00.7522	14 55 18.5	-58 17 41	15	0.01(31)	N	N	N			
MGE328.1916-00.7829	15 58 46.7	-54 11 54	24	1.1(10)	?	?	Y			
MGE334.3288-00.7978	16 27 55.3	-49 59 30	40	0.40(30)	Y	Y	Y			
MGE353.9103+00.4858	17 28 21.7	-33 48 41	15	0.04(47)	?	N	N			
MGE355.2478+00.9935	17 29 52.3	-32 24 59	18	0.16(9)	?	N	-			
MGE355.4167+01.0342	17 30 09.1	-32 15 11	14	0.01(87)	?	N	-			
MGE355.5953-02.1285	17 43 20.0	-33 48 11	15	0.02(29)	-	-	N			
MGE355.8086+01.2344	17 30 22.8	-31 48 57	15	0.07(14)	?	N	-			
MGE355.8839-01.4270	17 41 12.1	-33 11 18	18	0.19(4)	?	N	Y			
MGE356.0998+00.7001	17 33 14.2	-31 51 52	18	0.06(18)	?	N	N			
MGE356.1447+00.0550	17 35 54.5	-32 10 35	25	0.44(19)	Y	N	?	8.9	GPSR5 356.144+0.053	Rad
MGE356.4537+00.8358	17 33 36.4	-31 29 37	15	0.12(12)	N	?	N			
MGE356.5084+01.0838	17 32 46.3	-31 18 46	24	0.32(5)	N	N	-			
MGE356.6408-00.5704	17 39 39.5	-32 05 33	15	0.24(12)	N	N	-			
MGE356.7168-01.7246	17 44 29.6	-32 38 11	18	0.60(3)	Y	N	Y	12.8	IRAS 17412-3236	IR
MGE356.7415+00.7421	17 34 42.4	-31 18 10	16	0.23(43)	N	N	N			
MGE357.8187+00.2875	17 39 11.7	-30 38 19	16	0.20(46)	N	N	-			
MGE357.9893+02.8341	17 29 44.7	-29 06 57	21	0.21(4)	-	-	?			
MGE358.0888-01.5465	17 47 08.4	-31 22 21	20	0.08(20)	N	N	N			
MGE358.1166+01.0764	17 36 50.8	-29 57 53	15	0.03(31)	N	N	N			
MGE358.1558+00.7594	17 38 10.8	-30 06 06	24	0.22(8)	N	N	-			
MGE358.2600+01.4563	17 35 43.6	-29 38 22	19	0.05(18)	N	N	N			
MGE358.5717+02.5207	17 32 24.1	-28 48 02	26	0.05(19)	-	-	N			
MGE358.5824+02.6873	17 31 47.4	-28 42 03	33	2.2(1)	-	-	Y	1.5	PK 358+02 5 ^b	PN
MGE358.6633-01.3135	17 47 35.8	-30 45 38	15	0.01(22)	N	N	N			
MGE358.9738-02.2830	17 52 13.1	-30 59 28	21	0.02(23)	-	-	?			
MGE359.1142-01.6065	17 49 50.6	-30 31 30	20	0.02(45)	?	N	?			
MGE359.4290-00.5034	17 46 13.7	-29 41 09	15	0.16(26)	?	N	-			
MGE359.4372-02.6997	17 54 59.1	-30 48 09	18	0.02(21)	N	N	?			
MGE359.5136-02.6056	17 54 47.1	-30 41 21	35	0.02(34)	?	N	?			
MGE359.6095-01.9211	17 52 16.2	-30 15 36	29	0.03(46)	N	?	?			
MGE359.8693+01.0316	17 41 18.1	-28 30 21	36	0.04(49)	N	N	?			
4: Two-lobed										
MGE000.7126+02.7811	17 36 38.4	-26 51 39	19	0.02(21)	-	-	N			
MGE000.9066+02.1503	17 39 29.9	-27 02 01	18	0.20(3)	-	-	?			
MGE001.0651+02.7431	17 37 37.7	-26 35 01	18	0.06(7)	-	-	-			
MGE001.0839+01.9163	17 40 48.7	-27 00 27	18	0.05(14)	N	N	N			
MGE003.4305-01.0738	17 57 42.5	-26 32 05	19	0.05(16)	N	N	N			
MGE003.8212+02.6722	17 44 20.1	-24 17 00	18	0.05(13)	-	-	N			
MGE004.0396-02.7139	18 05 26.2	-26 48 56	23	0.07(14)	-	-	-	7.1	PN G004.0-02.7	PN
MGE007.3587+01.7685	17 55 34.7	-21 42 39	16	0.36(2)	-	-	?	0.9	PN G007.3+01.7	PN
MGE007.6093+02.0988	17 54 53.7	-21 19 41	30	0.06(24)	-	-	N			
MGE008.1733+01.0914	17 59 51.1	-21 20 39	18	0.12(15)	N	N	N			
MGE008.8168+02.2819	17 56 48.7	-20 11 34	24	0.05(31)	-	-	-			
MGE016.1274+00.3327	18 18 51.6	-14 45 10	18	0.31(14)	N	N	?			
MGE019.8603-00.3579	18 28 33.4	-11 46 43	31	1.2(9)	Y	?	?	11.6	IRAS 18257-1148	IR
MGE030.8780+00.6993	18 45 12.0	-01 30 31	18	0.15(13)	N	N	N			
MGE031.3183+00.9958	18 44 56.9	-00 58 54	18	0.05(21)	N	N	N			
MGE039.5964+00.4751	19 01 56.3	+06 08 46	20	0.05(31)	?	N	N			
MGE042.7665+00.8222	19 06 33.6	+09 07 20	33	1.1(1)	Y	Y	Y	5.2	IRAS 19041+0902	IR
MGE334.1114+00.3789	16 21 47.3	-49 19 23	21	0.99(4)	Y	Y ^k	Y			

Table 1—Continued

Name	J2000 Coordinates		Diam.	F ₂₄	Detection Flags			SIMBAD Associations		
	α (h m s)	δ ($^{\circ}$ ' ")			(")	(Jy)	8 μ m Point (6)	8 μ m Ext. (7)	70 μ m Ext. (8)	Dist. (") (9)
(1)	(2)	(3)	(4)	(5)	(6)	(7)	(8)	(9)	(10)	(11)
MGE355.7638+00.1424	17 34 35.2	−32 26 58	16	0.28(10)	?	N	N	9.9	NGC 6383 33	*iC
MGE356.1617-00.5486	17 38 21.8	−32 29 10	18	0.05(38)	?	N	N			
MGE356.5146-01.3137	17 42 19.7	−32 35 35	33	0.18(16)	?	N	?			
MGE357.2784-02.6349	17 49 34.3	−32 37 38	18	0.04(30)	–	–	?			
MGE358.0815+00.8514	17 37 38.2	−30 06 55	15	0.29(5)	Y	N	N			
MGE358.2846-00.2593	17 42 29.8	−30 31 59	18	0.13(20)	?	N	–			
5: Filamentary										
MGE011.1805-00.3471	18 11 28.9	−19 25 29	260	33.(18)	?	N	?	22.6	SNR G011.2-00.3 ^b	SNR
MGE027.3891-00.0079	18 41 19.8	−04 56 06	250	21.(89)	?	?	?	9.9	LMH 31 ^b	SNR
6: Miscellaneous										
MGE003.7032-01.7927	18 01 06.2	−26 39 21	60	0.01(68)	–	–	N			
MGE038.7425-00.6986	19 04 33.5	+04 50 58	14	0.04(14)	Y	N	N			
MGE304.6649-00.0439	13 06 38.7	−62 51 52		0.32(99)	Y	N	N	2.5	M01-221	*
MGE305.3881+00.0804	13 12 52.5	−62 41 21	90	0.13(94)	Y	N	N			
MGE314.2378+00.9793	14 23 21.0	−59 51 34	63	0.11(99)	Y	Y	?			
MGE316.8732-00.5991	14 47 45.1	−60 17 02	15	0.04(18)	Y	Y	Y	7.0	[JKK2007] G2	G
MGE317.0392-00.4974	14 48 36.0	−60 07 13	18	0.08(15)	N	Y ^k	Y	23.7	[JKK2007] G1	G
MGE351.2381-00.0145	17 23 04.4	−36 18 20	40	0.41(28)	N	Y	Y			
MGE353.5188+01.5107	17 23 13.5	−33 33 44	21	0.11(13)	–	–	–			
MGE356.3395+02.0502	17 28 33.9	−30 55 23	14	0.03(18)	–	–	?			

^aAlthough cut off from the MIPS GAL and GLIMPSE coverage, an MSX 8 μ m source, associated with Wray 15-1680, lies at the center of the ring. IRAS 17173-3305 is likely associated with the NE rim, but cannot be confirmed due to lack of coverage

^bAs mentioned in the text, a number of objects have secondary identifications not yet associated as such in SIMBAD. These are:

MGE001.0178-01.9642: IRAS 17525-2903
MGE001.2124-02.0748: PHR J1756-2857
MGE001.6301-02.6875: V* V3987 Sgr
MGE003.5282+02.6745: IRAS 17405-2430
MGE009.4257-01.2294: IRAS 18081-2123
MGE011.1805-00.3471: PSR J1811-1926
MGE027.3891-00.0079: PSR J1841-0456
MGE060.4530+00.0712: IRAS 19425+2411
MGE313.3544+00.3123: IRAS 14147-6033
MGE318.9322+00.6959: IRAS 14538-5800
MGE349.7294+00.1747: IRAS 17146-3723
MGE353.5300+02.1882: IRAS 17173-3305
MGE354.5377+02.4713: IRAS 17189-3207
MGE358.5016-00.5048: IRAS 17408-3027
MGE358.5824+02.6873: F3R 18

^cFull name: OGLEII DIA BUL-SC39 4483

^dFull name: 2MASS J18393224-0544204

^eIRAS 18588+0350 is associated with the SE rim

^fIRAS 16254-7439 is associated with the SE rim

^gIRAS 16228-5014 is associated with the SW rim

^hIRAS 16278-4808 is associated with the NW rim

ⁱIRAS 15293-5602 may be associated with the SE rim

^jIRAS 18468-0109 may be associated with the WSW rim

^kExtended emission seen in all IRAC bands

^lExtended emission is partially saturated

^mCentral source is saturated

ⁿObject matched in White et al. (2005) catalog of compact Galactic radio sources

^oObject matched in MAGPIS (Helfand et al. 2006) catalog of Galactic radio sources